PERFORMANCE OF RC COLUMNS STRENGTHENED WITH FABRIC-REINFORCED CEMENTITIOUS MATRIX (FRCM)

by

Nour Al Huda Haitham Tello

A Thesis presented to the Faculty of the
American University of Sharjah
College of Engineering
In Partial Fulfillment
of the Requirements
for the Degree of

Master of Science in

Civil Engineering

Sharjah, United Arab Emirates

May 2021

Declaration of Authorship

I declare that this thesis is my own work and, to the best of my knowledge and belief, it does not contain material published or written by a third party, except where permission has been obtained and/or appropriately cited through full and accurate referencing.

Signed: Nour Al Huda Tello

Date: May 17th, 2021

Approval Signatures

We, the undersigned, approve the Master's Thesis of Nour Al Huda Haitham Tello

Thesis Title: Performance of RC Columns Strengthened with Fabric-Reinforced Cementitious Matrix (FRCM)

Date of Defense: May 20th, 2021.

Name, Title and Affiliation	Signature
Dr. Farid Abed, Professor, Department of Civil Engineering Thesis Advisor	
Dr. Tamer El Maaddawy, Professor, Department of Civil Engineering, UAE University Thesis Co-Advisor	
Dr. Sherif Yehia, Professor, Department of Civil Engineering Thesis Committee Member	
Dr. Maen Alkhader, Associate Professor, Department of Mechanical Engineering Thesis Committee Member	
Dr. Irtishad Ahmed, Head Department of Civil Engineering	
Dr. Lotfi Romdhane, Associate Dean for Graduate Affairs and Research College of Engineering	
Dr. Sameer Al-Asheh, Interim Dean College of Engineering	
Dr. Mohamed El-Tarhuni, Vice Provost for Research and Graduate Studies Office of Graduate Studies	

Acknowledgement

Above all, I thank Allah the almighty, the most gracious and merciful, for His endless blessings and mercy, and for granting me the strength and patience to get through this journey.

Second, I would like to express my deepest gratitude and thankfulness for my advisor, Dr. Farid Abed, for his continuous guidance, help and support in all aspects since the first day I met him four years ago. I would also like to greatly thank my co-advisors from outside AUS, Dr. Ahmed El Refai from Laval University, and Dr. Tamer El Maaddawy from the United Arab Emirates University for continuously helping me and providing their invaluable guidance through my master's degree.

Furthermore, I would like to thank Dr. Sherif Yehia and Dr. Maen Alkhader for accepting to be committee members for my thesis, and for their helpful and insightful feedback. I would also like to thank the civil engineering lab instructor at AUS, Mr. Arshi Faridi, and the civil engineering lab technician, Mr. Mohammed Ansari, for their assistance in conducting all experimental lab work. Special thanks to my colleague and research assistant Yazan Al Houbi, for his greatly appreciated hard work and dedication in helping me with all experimental work inside and outside of AUS, during a time of a global pandemic. I would like to thank again Dr. Farid Abed as well as the civil engineering department at AUS for their support through the Graduate Teaching Assistantship, which was a great asset in helping me complete my graduate degree.

Moreover, I would like to thank Emirates Stone Company in Sharjah, UAE, for their generosity in providing all needed concrete and steel materials used in this study, and for their services in preparing and casting all specimens. I would also like to thank RureGold Company in Milan, Italy, for providing all the needed PBO-FRCM materials, as well as their assistance in the strengthening procedures.

Finally, I express my sincere gratitude, appreciation and thankfulness for my parents, siblings, extended family, as well as my precious friends, for their constant support and encouragement during my years of graduate studies at AUS. They are the greatest gift Allah has granted me, and I will forever strive to return the favor, and make them proud.

Dedication

To my beloved aunt Maha Tello…

Abstract

A recently emerging technique to strengthen existing concrete structures using Fiber-Reinforced Cementitious Matrix (FRCM) is introduced to retrofit structural members. FRCM is an inorganic matrix that consists of textile layers sandwiched between cementitious mortar layers. The main objective of this study is to investigate the response of reinforced concrete (RC) short columns strengthened with poly-paraphenylene-ben-zobisoxazole (PBO) FRCM under pure axial compression. The aim is to study the effect of the column cross-section shape as well as the number of FRCM layers on the effectiveness of PBO-FRCM systems in improving the strength and ductility of pre-damaged and non-damaged RC columns. A total of 10 columns with a clear height of 800 mm and a longitudinal reinforcement ratio of 1.5% were cast and tested monotonically until failure. Also, columns were either unwrapped which served as controls, wrapped with 2 PBO-FRCM layers or wrapped with 4 PBO-FRCM layers. Experimental results showed that strengthening pre-damaged RC columns with PBO-FRCM is highly efficient in restoring and increasing the original capacity, where the capacity increased with the increase of number of PBO-FRCM layers. Circular columns showed a better improvement in ultimate capacity where the capacity increase ranged from 38 to 71%. Also, strengthening short RC columns with PBO-FRCM increased the column ductility with a range of 19 to 82%. Finally, theoretical ultimate capacities of strengthened columns calculated using the provisions of ACI 549.4R-13 code showed that the code is accurate at estimating the capacity of short RC columns strengthened with PBO-FRCM.

Keywords: Reinforced concrete, RC columns, short columns, FRCM, PBO-FRCM, concrete strengthening, ultimate capacity, ductility

Table of Contents

Abstract…. 6

List of Figures 10

List of Tables 12

List of Abbreviations 13

Chapter 1. Introduction 14

1.1. Overview 14

1.2. Thesis Objectives 16

1.3. Research Contribution 17

1.4. Thesis Organization 17

Chapter 2. Background and Literature Review 19

2.1. FRCM Characteristics 19

2.2. Masonry 22

2.3. Beams 24

2.4. Columns 28

Chapter 3. Pilot Study 33

3.1. Experimental Program 33

3.1.1. Test matrix. 33

3.1.2. Design of test specimens. 33

3.1.3. Materials…. 35

3.1.4. Test setup and instrumentation. 36

3.2. Test Results and Discussion 37

3.3. Modifications Carried Forward for the Main Study 40

Chapter 4. Experimental Program 42

4.1. Test Matrix 42

4.2. Design of Test Specimens 42

4.3. Material Properties 46
4.3.1. Steel 46
4.3.2. Concrete 46
4.3.3. PBO-FRCM. 48
4.4. Pre-Damaging Stage 50
4.5. PBO-FRCM Installation 51
4.5.1. Surface preparation. 52
4.5.2. Mortar and mesh preparation. 52
4.5.3. Wrapping 53
4.6. Test Setup and Instrumentation 55
Chapter 5. Experimental Results 57
5.1. Axial Capacity 57
5.2. Axial load versus Displacement 58
5.3. Load-Strain Relationships 60
5.3.1. Load versus longitudinal steel strain. 60
5.3.2. Load versus middle tie strain. 61
5.3.3. Load versus longitudinal concrete strain. 61
5.3.4. Load versus transverse concrete strain. 62
5.4. Failure Modes 66
5.4.1. Group A 66
5.4.2. Group B 68
Chapter 6. Discussion of Results 71
6.1. Effects of Test Parameters on the Overall Behavior of PBO-FRCM Strengthened RC Columns 71
6.1.1. Effect of cross-section. 71
6.1.2. Effect of number of PBO-FRCM layers. 72
6.1.3. Effect of pre-damaging. 73

6.2. Analytical Prediction of Ultimate Capacity 74
6.3. Performance-Based Changes and Modifications from the Pilot Study 76
6.4. Comparison of Experimental Results with Previous Work 77
Chapter 7. Conclusion and Future Work 80
References 82
Vita 87

List of Figures

Figure 1: FRCM application steps. 16
Figure 2: Longitudinal cross-section of (a) square and (b) circular columns. 34
Figure 3: Cross-section of (a) square and (b) circular columns. 35
Figure 4: Pilot study specimen instrumentation. 36
Figure 5: Pilot study failure modes of (a) control columns, (b) columns strengthened with 1 PBO-FRCM layer, (c) columns strengthened with 2 PBO-FRCM layers and (d) columns strengthened with 4 PBO-FRCM layers. 38
Figure 6: Comparison between the ultimate capacity of square and circular columns of the pilot study. 39
Figure 7: Load versus longitudinal reinforcement strain of (a) square and (b) circular columns. 39
Figure 8: Load versus vertical concrete/ FRCM strain of (a) square and (b) circular columns. 39
Figure 9: Load versus horizontal concrete/ FRCM strain of (a) square and (b) circular columns. 40
Figure 10: Longitudinal cross-section of (a) Group A and (b) Group B columns. 44
Figure 11: Cross-section of (a) square and (b) circular columns. 45
Figure 12: End corbels cross-section of (a) square and (b) circular columns. 45
Figure 13: Stress versus strain for rebar samples of size (a) 10 mm and (b) 12 mm. 46
Figure 14: (a) Square columns, (b) circular columns and (c) end corbels steel cages. 47
Figure 15: Formwork used to cast (a) square and (b) circular columns. 48
Figure 16: Cast specimens. 48
Figure 17: Sample of PBO-FRCM provided by RureGold. 49
Figure 18: Pre-damaged columns after unloading. 51
Figure 19: Load versus strain for pre-damaged columns during pre-damaging. 51
Figure 20: Square columns edges (a) during grinding and (b) after grinding. 52
Figure 21: Mortar mixing process. 53
Figure 22: Mesh preparation process. 53
Figure 23: PBO-FRCM installation process. 55
Figure 24: Strain gauge installation on rebars. 56
Figure 25: Test setup and instrumentation schematics. 56

Figure 26: Load versus displacement for (a) control and (b) pre-damaged columns in Group A. 59
Figure 27: Load versus displacement for (a) control and (b) pre-damaged columns in Group B. 60
Figure 28: Load versus reinforcement bar strain for (a) Group A and (b) Group B. 63
Figure 29: Load versus middle tie strain for (a) Group A and (b) Group B. 64
Figure 30: Load versus vertical concrete strain for (a) Group A and (b) Group B. 65
Figure 31: Load versus horizontal concrete strain for (a) Group A and (b) Group B. 66
Figure 32: Group A failure modes. 68
Figure 33: Group B failure modes. 70
Figure 34: Ultimate capacity comparison between columns with different cross-sections. 72
Figure 35: Ultimate capacity comparison between columns wrapped with a different number of PBO-FRCM layers. 73
Figure 36: Ultimate capacity comparison between non-damaged and pre-damaged columns. 74

List of Tables

Table 1: Properties of fibers commonly used in FRCM fabrics. 16
Table 2: Summary of columns strengthened with FRCM literature review. 32
Table 3: Pilot study test matrix. 34
Table 4: Pilot study concrete properties. 35
Table 5: Pilot study test results. 37
Table 6: Summary of test specimen fabrication modifications applied on the pilot study's specimens for the use in the main study. 40
Table 7: Test matrix. 44
Table 8: Cylinders compressive strength. 47
Table 9: Properties of the PBO-FRCM bidirectional mesh according to the manufacturer's datasheet. 49
Table 10: Properties of the PBO-FRCM inorganic matrix according to the manufacturer's datasheet. 49
Table 11: Summary of experimental results. 57
Table 12: Experimental versus analytical results. 76
Table 13: Summary of comparison between main study and previous work. 79

List of Abbreviations

B-FRCM	Basalt Fiber-Reinforced Cementitious Matrix
C-FRCM	Carbon Fiber-Reinforced Cementitious Matrix
CFRP	Carbon Fiber-Reinforced Polymer
DS	Direct Shear
FEM	Finite Element Modeling
FRCM	Fiber-Reinforced Cementitious Matrix
FRP	Fiber-Reinforced Polymer
G-FRCM	Glass Fiber-Reinforced Cementitious Matrix
ICCP	Impressed Current Cathodic Protection
ICCP-SS	Impressed Current Cathodic Protection and Structural Strengthening
LVDT	Linear Variable Displacement Transducer
MB	Modified Beam
PBO	Poly-Paraphenylene-Ben-Zobisoxazole
PBO-FRCM	Poly-Paraphenylene-Ben-Zobisoxazole Fiber-Reinforced Cementitious Matrix
RC	Reinforced Concrete
S-FRCM	Steel Fiber-Reinforced Cementitious Matrix
SS	Structural Strengthening
TSR	Transverse Steel Reinforcement
UTM	Universal Testing Machine

Chapter 1. Introduction

In this chapter, an overview of the investigated problem is presented where the history of strengthening reinforced concrete (RC) structures and the introduction of the use of Fiber-Reinforced Cementitious Matrix (FRCM) are explored. The thesis objectives, research contribution and thesis organization are also explained.

1.1. Overview

The Arabian Gulf region has been rapidly developing in the areas of infrastructure and construction for the past decades. In most structures, RC has been mainly used. The Arabian Gulf region experiences harsh weather conditions for more than half the year, where the temperature reaches very high levels, and the humidity is excessive. Also, the region's exposure to seacoasts causes the coastal structures to be directly exposed to carbonation and chloride attacks. The aforementioned environmental conditions cause corrosion in the steel of RC, leading to a major loss in the capacity of structures, as well as a loss in ductility in the reinforcing bars that may lead to sudden failure by rupture, which is very dangerous. Furthermore, parts of the Gulf region lie in a seismic zone and are under the threat of possible seismic attacks. However, seismic loading considerations specified by the current RC design codes were not accounted for in most of the older constructed structures, which may cause catastrophic failure of structures in case of a strong earthquake.

The process of RC structures rehabilitation can be very expensive and unconventional, leading the industry to be constantly looking for less expensive and more convenient alternatives. In the past, repairment was done by RC jacketing, which is a procedure mainly based on the replacement of corroded steel bars by new bars and the removal of deteriorated concrete layers and replacing them by casting new concrete [1]. Another technique that has emerged in the past is wrapping deteriorated structures with strengthening materials such as Fiber-Reinforced Polymers (FRP's) [2]–[14].

FRP's are the most popular materials used for RC strengthening nowadays. They come in sheets of carbon, glass or basalt and are installed on the concrete surface by the use of epoxy, which is a very strong binder. The most advantageous property of FRP's is that they do not corrode, where corrosion is the main disadvantage of conventional steel. FRP's are also low in density and have a high strength to weight

ratio. However, FRP's are poorly compatible with the concrete substrate, poor in fire resistance and prone to debonding at high temperatures. Also, the used epoxy to attach FRP to the concrete surface has a toxic nature and poor thermal compatibility to the concrete substrate, as epoxy debonds in high temperatures.

Another strengthening technique has been recently introduced as an alternative to wrapping with FRP's, and that is strengthening using FRCM. FRCM consists of two components: fabric and mortar. The fabric can come in different materials such as carbon, glass and poly-paraphenylene-ben-zobisoxazole (PBO). The properties of different common FRCM fabric materials are summarized in Table 1. FRCM fabric also comes in steel and basalt, but those are less common. The fabric mesh can be in one direction or two directions where the spacing can be varied for each direction. Mortar is used as a binder to attach the fabric to the concrete surface. To install FRCM on any RC structure, the surface must be prepared properly. First, the surface must be repaired by casting new concrete if there was any deterioration in the original concrete. Then, the surface must be cleaned and wetted. After that, the first layer of mortar is applied with a thickness of a few millimeters. The first layer of fabric is then embedded into the mortar, where a certain overlapping length must be ensured. Between each two fabric layers, another layer of mortar must be added. The last layer of FRCM must always be mortar. The simplified process is shown in Figure 1.

FRCM has numerous qualities other than being non-corrosive that make it attractive to researchers, such as its extremely low weight-to-strength ratio, high tensile strength, ease of application on RC structures due to the binding agent being well-matched with the original concrete substrate, ability to resist extremely high temperatures, capability of maintaining the original stiffness of the strengthened structures and ability to include recycled materials.

ACI 549.4R-13 [15]; the guide to design and construction of externally bonded FRCM systems for repairing and strengthening concrete and masonry, includes guidelines for design, storing and installation of FRCM systems, but it does not predict the mode of failure of FRCM strengthened structures. Previous research has shown that FRCM can fail in three different ways, which are debonding at the matrix/substrate interface, delamination at the matrix/fabric interface or tensile rupture of FRCM material [16]–[19].

Table 1: Properties of fibers commonly used in FRCM fabrics.

Fiber filament properties	AR glass	Carbon	PBO
Density (g/cm^3)	2.50	1.74	1.56
Tensile strength (GPa)	1.28	3.79	5.80
Modulus of elasticity (GPa)	72	230	270
Ultimate deformation	0.018	0.016	0.025
Breakdown temperature (^oC)	1250	2500	650
Coefficient of thermal dilation, ($10^{-6}\ ^oC^{-1}$)	0.52	-0.01	-6.00

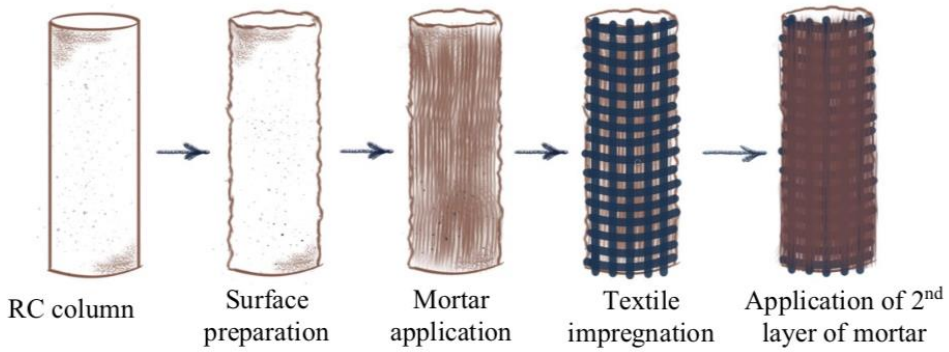

Figure 1: FRCM application steps.

1.2. Thesis Objectives

In this study, a test matrix was prepared to investigate the behavior of short RC columns wrapped with PBO-FRCM by varying a number of parameters and comparing the results to the ones acquired from un-wrapped control specimens. The parameters investigated included column's cross-section, the existence of pre-damaging or not and the number of PBO-FRCM layers. A monotonic loading test was conducted on all specimens where the applied load increased incrementally until the ultimate load was reached for the pre-damaging phase, or failure occurred in the columns for the reloading phase. The objectives of this experimental study are summarized as follows:

- To investigate the behavior of RC short columns strengthened with PBO-FRCM under monotonic loading. The aim is to study the effect of PBO-FRCM strengthening on the strength and ductility of pre-damaged short RC columns.
- To study the effectiveness of PBO-FRCM in improving the strength and ductility of circular versus square cross-sectional RC columns.

- To study the effect of the number of PBO-FRCM layers on the load capacity and ductility of pre-damaged short RC columns.
- To validate the analytical model suggested by the ACI 549 committee with the experimental results obtained from this study.

1.3. Research Contribution

RC structures are constantly prone to damage due to various external conditions such as corrosion and seismic loading. For many years, researchers have been investigating repair options due to this issue. Strengthening RC structures by FRP wrapping has been widely studied and implemented. Epoxy is used as a bonding agent between the concrete surface and the externally bonded FRP sheets. FRP sheets have proven to be very effective in strengthening existing RC structures. However, the epoxy used to bind the FRP sheets to concrete is flammable and prone to deterioration due to its mechanical and bond properties at high temperatures, as it is non-fire resistant. This property of epoxy is of great concern if the FRP wrapping technique is to be used in the Gulf region where the temperature is high throughout the year. Moreover, the epoxy used has a toxic nature adding another concern to using it.

This study proposes an alternative method to strengthening RC structures by FRP wrapping, and that is strengthening RC structure by FRCM wrapping instead. This new technique is similar to the older FRP wrapping technique where sheets of fiber are used to wrap the structural element. However, the binding agent used in this technique is cement-based mortar instead of epoxy, which acts as a barrier against chloride ions penetration thus protecting the main reinforcing bars from corrosion attacks. Furthermore, the fabric layers in this technique are completely embedded within the mortar, making the FRCM system fire resistant. This would make the use of FRCM systems more favorable than epoxy bonded FRP systems. Another appealing advantage of using FRCM systems is that the compatibility between the mortar and concrete substrate is inherited since both materials have cement as a common base.

1.4. Thesis Organization

This thesis is divided into 7 chapters following the abstract. Chapter 1 is the introduction where an overview of the topic, thesis objectives and the contribution of this thesis to research are presented. Chapter 2 includes a literature review where studies conducted on FRCM composites, masonry, beams and columns strengthened with

FRCM are showcased. Following the literature review, Chapter 3 presents a pilot study conducted prior to the main experiment of this thesis along with all of its results. Chapter 4 is the experimental program that consists of the test matrix, design of specimens, materials, PBO-FRCM installation procedure and test setup and instrumentation. After that, Chapter 5 and 6 present the results and discussion of results, respectively. Finally, Chapter 7 presents the conclusions and recommendations for future work.

Chapter 2. Background and Literature Review

In this chapter, a number of previous experiments conducted by researchers to study the characteristics of different FRCM systems are discussed. Additional studies that investigated the effect of strengthening masonry, RC beams and RC columns are presented as well.

2.1. FRCM Characteristics

Several studies were conducted on the bond characteristics of different FRCM systems [16], [17], [19]–[24]. Also, some experiments investigated how different external conditions such as curing and harsh environment affect the behavior of different FRCM systems [22], [23]. Other researchers explored how the technique of strengthening with FRCM can be integrated with other existing techniques to protect concrete structures from corrosion [24].

Younis and Ebead [17] studied the bond characteristics of carbon FRCM (C-FRCM), PBO-FRCM and glass FRCM (G-FRCM). Tensile tests were performed on all 3 types of FRCM, and the modulus of elasticity was calculated using the test results. Tensile tests were conducted on C-FRCM, PBO-FRCM and G-FRCM samples. G-FRCM specimens showed the most brittle behavior failing by fabric rupture. C-FRCM and PBO-FRCM failed by fabric slippage. After that, 18 prisms were cast with concrete and later wrapped with FRCM. A double shear test was conducted on the prisms to study the mode of failure, bond capacity and deformation of the wrapped specimens. The parameters varied were the mesh type, bond length and number of fabric plies. Bond length was not varied for G-FRCM due to its failure by rupture under the tensile test. Specimens wrapped with C-FRCM all failed by debonding within the matrix due to the bidirectional geometry of the mesh where the fabric in both directions had the same density, which caused the bond with the mortar to be weaker. Almost all PBO-FRCM wrapped specimens failed by debonding between the matrix and concrete as the bond within the matrix was very strong due to the fabric being denser in the wrap direction. For higher bond lengths, PBO-FRCM wrapped specimens failed by matrix rupture as the bond between the matrix and concrete became stronger. G-FRCM wrapped specimens failed by matrix rupture. PBO-FRCM wrapped specimens had the highest bond capacity, followed by C-FRCM and G-FRCM.

Kim et al. [19] investigated the bond characteristic between the matrix and textile within FRCM composites. Carbon and basalt textiles were used in this study where the matrix in the FRCM composites was developed with alkali resistance to increase the bond strength. Pull-out tests were performed to evaluate the bond characteristics between the matrix and textile within FRCM. Also, pull-off tests were conducted to evaluate the pull-off bond performance at the matrix-textile interface. Pull-out test results showed that C-FRCM had a higher bond strength and elastic modulus than basalt FRCM (B-FRCM) by around 169% for both properties. Also, pull-off test results showed that C-FRCM had the best bond performance complying with the pull-out test results.

Another study on C-FRCM was conducted by Zhu et al. [20] where the bond behavior of C-FRCM within the matrix at the fabric-mortar interface was studied. Bidirectional C-FRCM fabric was used in this study. An asymmetric configuration was used for the test setup where an upper cut intercepted carbon yarn in the middle and two additional cuts kept the middle carbon yarn intact. Each specimen had an upper and a lower block where the lower block's anchorage length was longer to provide sufficient and strong anchorage. Each specimen was clamped on both ends and each specimen end was reinforced with carbon FRP (CFRP) sheets to avoid local failure. All specimens underwent a displacement-controlled pullout test where the loading rate was 0.2 mm/min. Test results showed that specimens with lower upper block lengths failed purely due to slippage of carbon yarn, and specimens with higher upper block lengths failed due to slippage accompanied with partial rupture of carbon yarn.

The bond between PBO-FRCM strengthening materials and concrete was studied by D'Ambrisi et al. [16]. The bond length and number of FRCM layers were varied across the specimens. A double face shear test was conducted on all specimens. Test results have shown that the specimens failed due to debonding at the fibers interface followed by matrix rupture. Also, the ratio of the debonding strain was independent of the bond length.

Calabrese et al. [21] used direct shear (DS) and modified beam (MB) tests to study the effect of interface normal stresses on the bond behavior of FRCM composites. C-FRCM and PBO-FRCM were used to strengthen a masonry substrate. For the MB tests, two specimen geometries were used; one where the number of bricks in each

masonry unit was equal to 1 and another one where it was equal to 3. Both geometries had two composite strip layouts. Both types of tests were conducted monotonically in displacement control using an electro-mechanic testing machine where the rate was 0.204 mm/s. Results showed that due to the presence of a normal stress component for specimens that underwent the MB tests, the axial stress increased, and the global slip of MB tests decreased in comparison with the DS tests. For PBO-FRCM strengthened specimens, the maximum difference of average peak axial stress and corresponding global slip was around 9 and -69%, respectively. For C-FRCM strengthened specimens, the maximum difference was around 38 and -33%, respectively.

Wang et al. [22] investigated how the tensile behavior of FRCM composites is affected by the curing conditions of the cementitious mortar. Cement paste cylinders with a diameter of 50 mm and a height of 100 mm were cast. Also, steel FRCM (S-FRCM) composites and the same mortar used for the cubes were used to cast coupons. To investigate the curing conditions effect, the specimens were separately placed in climatic chambers where each one had different curing conditions. Temperature, humidity level and curing time were varied for each chamber. Also, some of the samples were immersed in water while other samples were exposed to air. Split tensile tests and direct tensile tests were conducted on the cylinders and coupons, respectively. Results showed that hydration of cement was the main factor of strength development as tensile strength was the highest for specimens that were cured in water and had the highest degree of hydration. Also, coupons cured under high temperature and humidity conditions had higher absolute stresses.

Donnini et al. [23] studied the effect of exposure to harsh environments on the mechanical behavior of the fabric, mortar and composite system of G-FRCM. G-FRCM was subjected to different harsh environment conditions such as saline, alkaline and freeze-thaw cycles. To investigate the mortar behavior, 3 prisms were cast for each type of environmental conditioning. To investigate the fabric behavior, 5 glass yarns were subjected to displacement-controlled tensile tests at a loading rate of 0.5 mm/min. To investigate the composite system behavior, 20 G-FRCM coupons were subjected to displacement-controlled direct tensile tests at a loading rate of 0.5 mm/min as well. Results showed that environmental conditioning had almost no effect on the behavior of the mortar. However, glass yarn was affected by environmental conditioning where

the tensile strength was reduced by around 25% under alkalinity conditions and by around 8% under salinity and freeze-thaw conditions. G-FRCM coupons were barely affected by the environmental conditioning due to the presence of the inorganic matrix. All G-FRCM coupons failed by rupture of the glass yarn under all environmental conditions.

Su et al. [24] introduced the technique of combining impressed current cathodic protection and structural strengthening (ICCP-SS) for repairing concrete structures damaged by chloride-induced corrosion. The technique's effect on the flexural strength, compressive strength, conductivity and shear strength was studied. The type and amount of high molecular weight polymer used were varied. The amount of chopped carbon fiber and impressed current density were varied as well. 7 specimens were cast where one of them was acting as control, 3 of them had re-dispersible polymer powder and the other 3 specimens had styrene butadiene latex. Results showed that using chopped carbon fibers provided a cathodic protection for the reinforcement in the structures. Furthermore, it was observed that as the current density increased, the shear strength between the C-FRCM and concrete substrate decreased due to the anodic polarization. Also, the impressed current cathodic protection technique (ICCP) was found to be capable of providing effective cathodic protection for reinforcements.

2.2. Masonry

A number of studies was conducted on strengthening masonry structures with FRCM where researchers either conducted experimental studies [25], numerical studies [26] or both [27], [28] for the purpose of comparison and verification of the proposed finite element modeling (FEM) models.

Franzoni et al. [25] studied the mechanical behavior of solid fired-clay masonry bricks subjected to salt crystallization cycles after strengthening with S-FRCM. 1 layer of unidirectional S-FRCM was used to strengthen the masonry bricks. All masonry bricks were cured for 28 days after casting. To simulate the damage caused by salt crystallization cycles, bricks were subjected to artificial weathering protocol where specimens underwent cycles of wetting and drying. Also, specimens were either partially or totally wrapped with S-FRCM. Partial wrapping was conducted to study the effect of permeability on sulfate accumulation at the areas with no S-FRCM, while total wrapping was conducted to observe if S-FRCM would detach from the specimens due

to salt accumulation beneath the S-FRCM composite. Single lap shear tests were conducted on all specimens. Results showed that all specimens failed by S-FRCM delamination. Also, strengthening with S-FRCM did not cause any local salt accumulation between the composite and masonry face.

A numerical study was conducted by Turk [26] to analyze the effect of PBO-FRCM strengthening on the dynamic response of a natural stone block masonry minaret of a historical mosque located in Istanbul, Turkey. FEM was used to conduct the analysis where seismic loads were applied for 2 different artificial accelerograms and the maximum lateral displacement at the top of the minaret was obtained by using time history analysis. Analysis was conducted on the model with and without PBO-FRCM strengthening. Results showed that PBO-FRCM strengthening reduced the lateral displacement by around 38%.

Carozzi et al. [27] conducted experimental and numerical studies to investigate the behavior of single bricks and small masonry pillars strengthened with G-FRCM. The parameters varied were the bond length, type of mortar and type of bricks. Tensile tests were performed for the weft and wrap directions. Experimental results showed that the use of cementitious-based mortar was more efficient than the use of limestone-based mortar, as the former type showed a 54% increase in strength as the bond length increased compared to the latter type that showed a 15% increase only. 2 types of FEM models were modeled and analyzed. In the first model, only the FRCM composite was modeled using 1D Finite Elements where in the second model, a fully 3D Finite Element approach was considered. Numerical analysis results of both models concluded that both approaches can be used for future design considerations.

Murgo and Mazzotti [28] conducted experimental and numerical experiments as well to evaluate the structural behavior of masonry columns strengthened with FRCM. 1 layer of C-FRCM and G-FRCM was used to wrap masonry columns either continuously or discontinuously. Uni-axial compression tests were conducted on all specimens. Experimental results showed that the increase in compressive strength was very low as the ratio between the compressive strength of the columns strengthened with C-FRCM and the control unstrengthened specimen was 1.085, while it was 1.055 for the columns strengthened with G-FRCM. This was attributed to the small amount of external C-FRCM reinforcement used compared to the relatively big size of the

column. A 1D Finite Element model was used to simulate the experiment where results showed the model to be accurate.

2.3. Beams

Numerous studies were conducted to study the flexural behavior of RC beams strengthened with different FRCM systems under monotonic loading or fatigue [29]–[31]. Furthermore, some researchers investigated the effect of strengthening RC beams subjected to corrosion with different FRCM systems [32]. Other studies were conducted on the shear behavior of RC beams strengthened with different FRCM systems using different shear-strengthening schemes [33]–[37]. Also, other studies explored the shear behavior of RC beams strengthened with FRCM experimentally and analytically and later compared both sets of results [38], [39].

Jabr et al. [29] investigated the effect of strengthening RC beams with different FRCM composites on the flexural capacity. 8 beams were cast where either PBO-FRCM, C-FRCM or G-FRCM was used for strengthening. Also, the number of FRCM layers as well as the steel reinforcement ratio were varied. According to the results obtained from the flexural tests, it was concluded that RC beams strengthened with PBO-FRCM resulted in the highest increase in ultimate capacity for both the low and moderate internal reinforcement ratios with a value of 33 and 25%, respectively. Furthermore, both C-FRCM and G-FRCM did not significantly impact the ultimate capacity due to the premature failure of FRCM. Moreover, it was noticed that as the increase in the ultimate strength decreased, the axial stiffness ratio decreased. C-FRCM showed the greatest increase in post-cracking stiffness which was 23% and increased the yielding load by 17%. FRCM also helped in reducing the crack width relative to the unstrengthened control beam.

Sneed et al. [30] studied the behavior of RC beams strengthened with S-FRCM. The varied parameters were the number of S-FRCM layers, U-wrap anchorage and the loading rate. 7 beams were cast and tested using a single-lap shear test. Based on the obtained results, it was concluded that lowering the concrete compressive strength or reducing the concrete cover decreased the load-carrying capacity. The failure of RC beams strengthened with S-FRCM was independent of both parameters and was solely governed by the fabric slippage within the matrix. Furthermore, it was noticed that corrosion had an insignificant effect on the mode of failure of S-FRCM-strengthened

RC beams. In addition, all beams strengthened with 2 and 4 layers had the same failure mode, which was delamination of the S-FRCM layer at the matrix interface regardless of the level of corrosion.

Akbari Hadad et al. [31] conducted a study on strengthening concrete beams with FRCM, where the beams were subjected to static loading and fatigue prior to strengthening. 2 different types of C-FRCM systems were used where the first one had bidirectional carbon mesh with equal spacing in both directions and the second one had unidirectional carbon mesh. All beams were designed to be under-reinforced. The number of C-FRCM plies was either 1 or 2. A three-point loading test was conducted on all specimens where the tests were in displacement control for static loading and in force control for fatigue. For static loading tests, no debonding was observed in any specimen and all strengthened beams sustained higher loads than the un-strengthened ones. The maximum increase in flexural capacity for the static loading tests was achieved by the beam strengthened with 2 layers of the unidirectional C-FRCM where the increase was around 35%. For fatigue tests, all specimens failed by steel yielding for the beams that failed before two million cycles. For the beams that did not fail before two million cycles, a monotonic test was conducted to find the residual strength and the results were compared with the static test results.

Elghazy et al. [32] investigated the performance of RC beams that were subjected to corrosion and later rehabilitated with PBO-FRCM. Corroded specimens were subjected to wet-dry cycles in a large environmental chamber. A 10% of steel mass loss was desired and achieved. The corroded specimens were later repaired using commercial cementitious repair mortar with a compressive strength higher than the original concrete used for casting. The specimens were wrapped with 1, 2 or 4 fabric plies, and two PBO-FRCM repair schemes were used: “UU” and “CU”. Both schemes had PBO-FRCM applied to the tension face, but for the UU scheme, one U-shaped transverse strip was bonded around the beam’s cross section as anchorage, and for the CU scheme, a continuous U-shaped ply was applied along the beam’s span. A four-point loading test was conducted on all specimens. All strengthened beams experienced concrete crushing after steel yielding. All UU scheme specimens failed by PBO-FRCM delamination except for the one reinforced with 4 plies which failed by PBO-FRCM

slippage at the end anchorage followed by PBO-FRCM delamination. All CU scheme specimens failed by slippage of fabric within the matrix.

Younis et al. [33] investigated the effect of strengthening RC beams in shear with different FRCM systems on the shear capacity. 16 beams were cast where the effect of a number of parameters was investigated. C-FRCM, PBO-FRCM or G-FRCM was used to strengthen the specimens. Also, continuous or discontinuous strips were used for strengthening where the inclination angle was varied for discontinuous strips. A three-point loading test was conducted on all specimens to investigate shear behavior. Test results showed that the average capacity increase was around 51%, the mode of failure for all beams was FRCM debonding and anchorage had an insignificant effect on the strength.

Younis et al. [34] also investigated FRCM shear strengthening for RC beams. 7 shear-critical RC beams were cast where C-FRCM, PBO-FRCM or G-FRCM was used for strengthening. Also, the strengthening scheme was either a single full length FRCM plate or a set of intermittent and spaced FRCM strips. A three-point loading test was conducted on all specimens. Results showed that strengthening beams with FRCM in shear increased the capacity between 31 and 100%. Also, the full-length strengthened specimens increased the beam capacity more than the other strengthening technique did for each FRCM material. The highest strength increase was in the specimens strengthened with C-FRCM.

Azam and Soudki [35] studied the effect of strengthening RC beams with FRCM on shear capacity. 7 shear-critical beams were cast where C-FRCM or G-FRCM was used to strengthen the beams. The strengthening scheme was either side bonded or U-wrapped. All specimens were tested under three-point bending. Test results showed that FRCM strengthening was effective in enhancing the load-carrying capacity of shear-critical RC beams. The increase in load-carrying capacity of the FRCM-strengthened beams ranged between 19 and 105%. Also, it was shown that both strengthening schemes showed a similar behavior. The obtained results indicated that the bond between FRCM and the concrete surface was perfect, and thus the use of anchorage could be neglected. Furthermore, FRCM strengthening increased the stiffness of the beams where the increase in stiffness ranged between 9 and 11% relative to the control specimens.

Loreto et al. [36] evaluated the behavior of RC beams strengthened in shear with PBO-FRCM. The varied parameters were the type of concrete and number of PBO-FRCM layers. 6 beams were cast where 5 of them were strengthened with FRCM U-wraps and the sixth beam served as control. Three-point loading tests were conducted where the results showed that shear strength increased with the increase of the number of FRCM layers but not linearly. Also, the failure mode depended on the number of FRCM layers, as one-layer strengthened beams failed by slippage of the fabric within the matrix while the four-layers strengthened beams failed by delamination.

Aljazaeri and Myers [37] presented an experimental study on the behavior of RC beams externally strengthened in shear with PBO-FRCM. Some specimens had internal transverse shear reinforcement while others did not. Vertical PBO-FRCM U-wrap sheets were used to strengthen the beams where some of the beams were continuously wrapped, and some were partially wrapped. All beams were tested under a four-point loading test. Results showed that beams with internal transverse reinforcement showed a significant increase in shear capacity due to strengthening with PBO-FRCM where the maximum percentage increase was around 32%. However, beams with no internal transverse reinforcement did not show a significant capacity increase. Continuous U-wraps provided a more desirable ductile failure.

Marcinczak et al. [38] studied the effect of shear strengthening of RC beams with PBO-FRCM with anchorage on the shear capacity. The results were later compared with theoretical calculations performed using the ACI 549 code. 10 RC T-beams were cast and strengthened with PBO-FRCM with 3 different anchorage systems. All beams were partially wrapped with PBO-FRCM strips. Three-point loading tests were conducted on all beams. Test results showed that there was no need for anchorage to prevent premature debonding of the mesh as slippage occurred between the fibers and matrix of the PBO-FRCM system. Also, comparisons between experimental and analytical results showed that the ACI 549 code is highly conservative especially for beams with anchorage.

Akbari Hadad et al. [39] investigated the flexural behavior of RC beams strengthened with C-FRCM and compared the experimental results with analytical ones. Concrete of different compressive strengths was used to cast the specimens. Also, specimens were either unstrengthened, strengthened with 1 C-FRCM ply or

strengthened with 2 C-FRCM plies. All beams were tested monotonically under four-point bending in displacement control where the loading rate was 5 mm/min. Experimental results showed a capacity increase of 58 and 86% for the specimens cast with low strength concrete and strengthened with 1 and 4 C-FRCM plies, respectively. Also, results showed a capacity increase of 57 and 96% for the specimens that had a higher concrete strength and strengthened with 1 and 4 C-FRCM plies, respectively. The percentage difference between experimental and analytical results was between -4 and 15%.

2.4. Columns

Various studies were conducted on the behavior of concentrically [40]–[45] and eccentrically [18], [46] loaded RC columns strengthened with different FRCM systems. In those studies, different parameters were varied such as but not limited to subjecting specimens to pre-damage prior to testing or not, cross-section type, transverse reinforcement spacing, FRCM system type and number of FRCM system layers. Table 2 summarizes the experimental programs and main results of all the previous studies conducted on columns that are mentioned in this literature review.

An experimental study was conducted on cylindrical specimens and square prisms strengthened with PBO-FRCM by Colajanni et al. [40]. In this study, the length of specimens, type of cross-section, reinforcement ratio, number of FRCM layers and overlapping length were varied in order to study their effect on capacity and ductility. A standard monotonic loading test was conducted on all specimens. Results showed an increase in strength and ductility depending on the number of FRCM layers as well as the overlapping length. Also, specimens that had a square cross-section showed an improvement in strength after wrapping, which was unexpected. The maximum increase in capacity was achieved by the cylindrical specimen confined with 3 PBO-FRCM layers where the increase was around 64%. All cylindrical specimens failed by FRCM rupture after formation of wide vertical cracks in the FRCM textile, while prism specimens failed by FRCM rupture at the corners. A mathematical model was produced using the results of the study.

Colajanni et al. [41] studied the behavior of cylindrical and prismatic specimens wrapped with C-FRCM under monotonic and cyclic loading by varying the cross-section, number of C-FRCM layers and corner radius of prismatic specimens. All

specimens had an overlapping length of 100 mm. Results showed that C-FRCM provided considerable strength gain and ductility improvement for all specimens, and the maximum gain was in cylindrical specimens with a maximum value of around 49%. Increasing the number of C-FRCM layers increased the strength gain but decreased the ductility for all specimens. C-FRCM installation was effective for prismatic specimens that had a cross-section with an aspect ratio of 2, as opposed to the prediction preceding the study. Varying the corner radius had a very small effect on the performance of wrapped specimens, but a noticeable effect on the wrapped prismatic specimens' strains.

Faleschini et al. [42] studied the axial behavior of RC columns strengthened with C-FRCM. 12 columns were cast where the cross-section was either circular or square with rounded edges. The columns were either unconfined to serve as control or confined with 1 or 2 C-FRCM layers. Also, the tie spacing was varied for the columns. All columns were tested under displacement-control where the loading speed was 0.3 mm/min. Results showed that square columns still had stress concentrations despite rounding the corners. Furthermore, the increase in number of plies increased the capacity, especially for the circular columns where the maximum increase was around 24%.

Feng et al. [43] investigated the behavior of corroded circular RC columns strengthened with C-FRCM under cyclic loading. 7 specimens with the same dimensions, concrete strength and reinforcement were designed and cast where 1 column was not corroded and served as a control specimen. To achieve corrosion, specimens were kept in water for 12 hours a day for a total of 360 days. To accelerate the process, 3% NaCl by cement weight in the concrete mix was used. Specimens were either wrapped with 2 or 3 C-FRCM layers. For cyclic testing, each column was loaded with a hydraulic actuator installed at the column cap horizontally with a capacity of 2000 kN and vertically with a capacity of 5000 kN. 3 displacement cycles were applied at loading amplitudes starting with 2 mm and increasing with an increment of 4 mm. The maximum capacity increase was around 33% and it was achieved by the specimen wrapped with 3 C-FRCM layers and was subjected to a high axial compression ratio.

Toska et al. [44] studied the effectiveness of repairing severely damaged RC columns by C-FRCM wrapping. The cross-section shape, transverse reinforcement

spacing, whether the specimen was pre-damaged or not and whether the specimen was wrapped with 2 C-FRCM layers or not were the parameters varied across the cast specimens. Pre-damaged specimens were damaged up to 70%. After damaging the specimens, the loose concrete was removed, and the original cross-section of the specimens was restored by applying mortar. After 28 days, the specimens were wrapped with 2 C-FRCM layers. All specimens were tested under axial loading in displacement-control mode where the loading rate was 0.3 mm/min. Results showed that C-FRCM strengthening restored the capacity of all damaged columns except the square column with the lower transverse reinforcement ratio where only 90% of the capacity was restored. The undamaged circular column strengthened with C-FRCM showed the highest capacity increase of around 34%. Also, pre-damaged specimens reached higher lateral strain levels than the undamaged ones.

Zhu et al. [45] studied RC columns confined with C-FRCM under ICCP-SS, which is a new intervention method used to rehabilitate sea-sand concrete columns. Sodium chloride (NaCl) was used to induce corrosion. 9 columns were cast and were divided into 5 groups. The first group included control columns, the second group included one column with NaCl and no repair, the third group included two columns with NaCl repaired by the ICCP technique without C-FRCM, the fourth group included one column with NaCl repaired by the structural strengthening (SS) technique only and the fifth group included 3 columns with NaCl repaired by ICCP-SS. After curing the columns, the ones with NaCl were exposed to accelerated corrosion for 270 days and the ones repaired by ICCP were exposed after that to cathodic protection for 250 days. All columns were tested under a compressive test. Results showed that the maximum capacity increase of retrofitted columns by ICCP-SS was around 37%. A confinement model was proposed using the results of this study.

A study on the behavior of eccentrically loaded PBO-FRCM strengthened concrete columns was conducted by Trapko [18]. The specimens were either un-wrapped, wrapped with PBO-FRCM horizontally or wrapped with PBO-FRCM horizontally and vertically. The horizontal layers were parallel to the column axis where vertical layers were perpendicular to the column axis. Prior to installing PBO-FRCM, the columns were cleaned, dusted and washed. An overlapping length of 100 mm was considered for each fabric layer. A compressive test was conducted on all specimens.

PBO-FRCM strengthening resulted in a capacity restoration ranging from 62 to 84%. Confinement in one direction showed better results than confinement in two directions. PBO-FRCM wrapping also showed to be less effective than FRP wrapping where epoxy is used as a binder.

Ombres and Verre [46] studied the structural behavior of rectangular concrete columns strengthened with PBO-FRCM under eccentric loading by varying the reinforcement ratio and eccentricity to height (e/h) ratio. 2 reinforcement ratios were used: 0.8 and 1.4%. For each reinforcement ratio, 3 columns were cast where one remained un-strengthened, one was strengthened with 1 PBO-FRCM layer, and one was reinforced with 2 PBO-FRCM layers. Eccentricity was varied for all columns. Before installing PBO-FRCM, the specimens were sandblasted after 28 days of casting concrete and were left in ambient environment for 7 days. All specimen corners were rounded to a radius of 20 mm. A compressive test was conducted on all specimens. All confined columns showed an increase in strength that varied between 20 and 39%. Strength gain increased with the increase in reinforcement ratio and decreased with the increase in (e/h) values.

In this study, the experimental program consisted of short square and circular RC columns that were cast with low strength concrete in order to simulate deficiency in concrete. To further weaken the columns, pre-damaging procedures were conducted on a number of the columns where the columns were monotonically subject to 100% of the ultimate capacity. This step will contribute to the literature since it was not conducted in any of the aforementioned previous studies. Another addition to the literature would be the use of 4 FRCM layers, which was also not seen in any of the previous studies. All columns were concentrically subjected to axial load up to failure.

Table 2: Summary of columns strengthened with FRCM literature review.

Reference	Test type	Pre-damage	No. of columns	$f'c$ (MPa)	Cross-section shape	Dimensions (mm x mm)	ρ_s (%)	Ties		e/D (%)	Type of FRCM system	No. of FRCM layers	Strength increase due to FRCM (%)
								Bar size (mm)	S (mm)				
Colajanni et al. [40]	M	No	9	25	C R	154x335, 200x335 200x200x425	0	-	-	0	PBO	0, 2, 3	2 to 64
Colajanni et al. [41]	M & Cy	No	30	17	C R	200x600 200x200x600, 200x400x600	0	-	-	0	Carbon	0, 2, 3	14 to 49
Faleschini et al. [42]	M	No	12	16	C R	300x1000 300x300x1000	0.68	8	200, 330	0	Carbon	0, 1, 2	0 to 24
Feng et al. [43]	Cy	Yes	7	44	C	300x1350	1.71	8	100	0	Carbon	0, 2, 3	15-33
Toska et al. [44]	M	Yes	9	21	C R	300x1000 300x300x1000	0.68	8	200, 330	0	Carbon	0, 2	-10 to 34
Zhu et al. [45]	M	Yes	9	42	C	220x660	1.78	8	150	0	Carbon	0, 1	-2 to 37
Trapko [18]	M	No	15	49	R	200x200x1500	1.13	6	170	0, 8, 16	PBO	0, 1, 2	-38 to -16
Ombres and Verre [46]	M	No	8	24, 40	R	150x150x900, 150x150x500	0.80, 1.40	6	100	12, 16, 18, 20, 33	PBO	0, 1, 2	20 to 39

$f'c$= concrete compressive strength; ρ_s= longitudinal steel reinforcement ratio; S= tie spacing, e/D= ratio between eccentricity and cross-section diameter or side dimension; M= monotonic loading; Cy= cyclic loading; C= circular; R= rectangular.

Chapter 3. Pilot Study

Prior to developing the experimental program and the execution of the main experiment, a pilot study was conducted to further understand the behavior of short RC columns strengthened with FRCM beyond the information obtained from the literature review. This pilot study was published in the Composite Structures journal in September 2020 [47]. In the pilot study, no pre-damaging procedures were conducted before PBO-FRCM strengthening. All the details regarding the experimental program, results, and analysis of results of the pilot study are presented in this chapter. Modifications were made to the fabrication of the test specimens for the main study based on the pilot study test results.

3.1. Experimental Program

3.1.1. Test matrix. A total of 8 columns were cast for the pilot study as shown in Table 3. The columns were divided into 2 main groups based on their cross-section, which was square or circular. Square columns were reinforced with 4 bars of 12 mm diameter while circular columns were reinforced with 6 bars of 10 mm diameter, unifying the reinforcement ratio for all columns which was 2%. For each group, 1 column was unstrengthened and served as a control specimen, 1 column was wrapped with 1 PBO-FRCM layer, 1 column was wrapped with 2 PBO-FRCM layers and 1 column was wrapped with 4 PBO-FRCM layers. The specimen numbering system consisted of the letter S or C denoting square and circular cross-section, respectively. The first letter was followed by the number of PBO-FRCM layers used to strengthen the specimen which was either 0, 1, 2 or 4.

3.1.2. Design of test specimens. All columns were designed to behave as short columns in order to study the pure axial behavior of loaded columns without the interference of any slight eccentric loading during the compressive tests. To do so, Equations 1 and 2 were used from the ACI 318-19 provisions [48] as will be later explained in Chapter 4. Furthermore, Equation 3 from the ACI 318-19 code [48] was used to determine the cross-sectional dimensions for columns based on the desired capacity. Square columns had a cross-section of 150x150 mm while circular columns had a cross-section diameter of 170 mm. All columns had a cross-section clear cover of 15 mm, and a total height of 800 mm. Figure 2 shows the longitudinal cross-section

of square and circular columns, respectively. Figure 3 shows the cross-section of square and circular columns, respectively. All columns were transversely reinforced with ties of 6 mm diameter at a spacing of 75 mm. A smaller tie spacing was used at both ends of the columns to reduce the possibility of columns failing prematurely at the concentrated loading points as shown in Figure 2.

Table 3: Pilot study test matrix.

Specimen	Reinforcement	Reinforcement ratio (%)	FRCM layers
Group 1: Square columns			
S0	4ϕ12	2	-
S1			1
S2			2
S4			4
Group 2: Circular columns			
C0	6ϕ10	2	-
C1			1
C2			2
C4			4

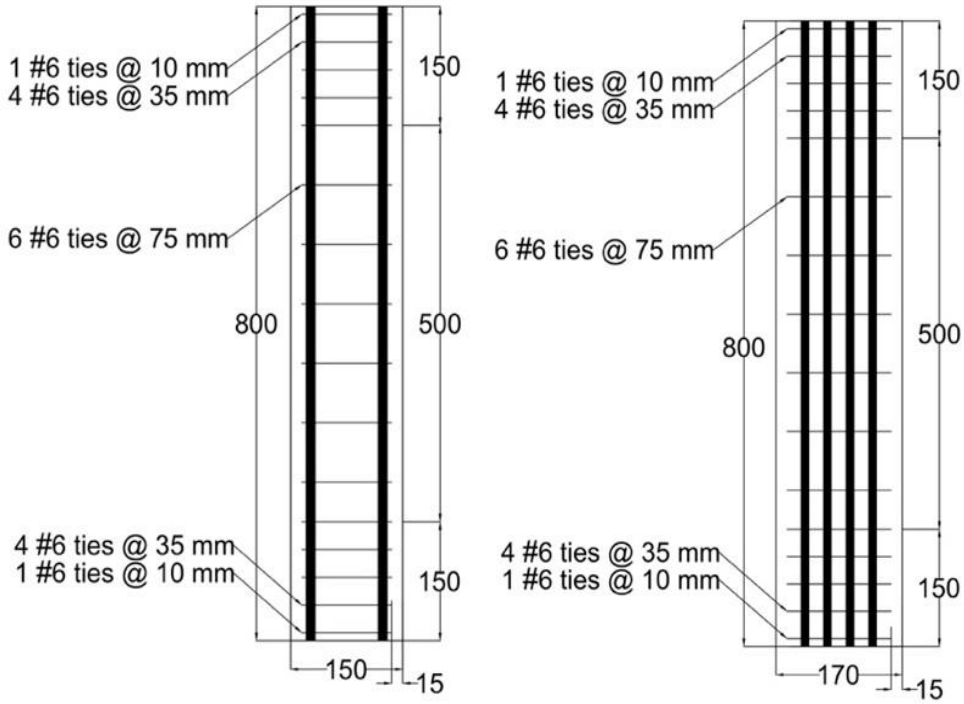

(a) (b)

Figure 2: Longitudinal cross-section of (a) square and (b) circular columns.

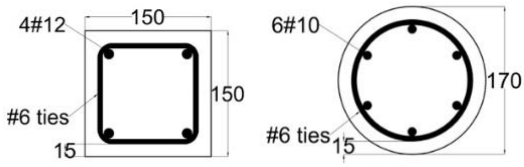

(a) (b)

Figure 3: Cross-section of (a) square and (b) circular columns.

3.1.3. Materials. All longitudinal and transverse steel used in the pilot study had the same mechanical properties as the steel used in the main study, where all details are presented in Chapter 4.

All columns were to be cast with concrete with a compressive strength of around 30 MPa. All columns were cast at Emirates Stone Company where the provided concrete had an average compressive strength of 31.7 MPa based on the results of conducting standard tests according to ASTM C39 [49] on 5 150x300 mm cylinders on the day of testing as shown in Table 4. Also, 4 150x150x150 cubes were cast with the columns and tested on the day of column testing according to BS1881-116:1983 [50]. Results showed a cube average compressive strength of 34.2 MPa as shown in Table 4.

Table 4: Pilot study concrete properties.

Specimen	Compressive strength (MPa)	Average compressive strength (MPa)
Cylinder 1	30.8	
Cylinder 2	30.9	
Cylinder 3	34.7	31.7
Cylinder 4	27.3	
Cylinder 5	34.7	
Cube 1	34.7	
Cube 2	33.2	34.2
Cube 3	35.5	
Cube 4	33.4	

PBO-FRCM used for wrapping in the pilot study was provided by RureGold Company. The mesh and cementitious matrix properties as well as the wrapping procedure are mentioned later in Chapter 4, since they were the same for the main study.

3.1.4. Test setup and instrumentation. Prior to casting, strain gauges were installed at the midpoint of 2 opposing rebars as well as the middle tie for each steel cage. After curing the specimens for 28 days and wrapping with PBO-FRCM, additional strain gauges were vertically and horizontally installed at the mid-height of the external column surface. Also, 2 linear variable displacement transducers (LVDT's) were installed at the columns' mid-height at opposing sides to measure the column vertical displacement during testing. Figure 4 shows the instrumentation of test specimens. All strain gauges and LVDT's were connected to a digital data acquisition system that records data at a rate of 600 readings/min. All columns were axially subjected to monotonic compressive tests where the loading rate was 0.3 mm/min. Columns were capped with steel caps at both ends to ensure the load was being distributed evenly across the cross-section of the column under testing.

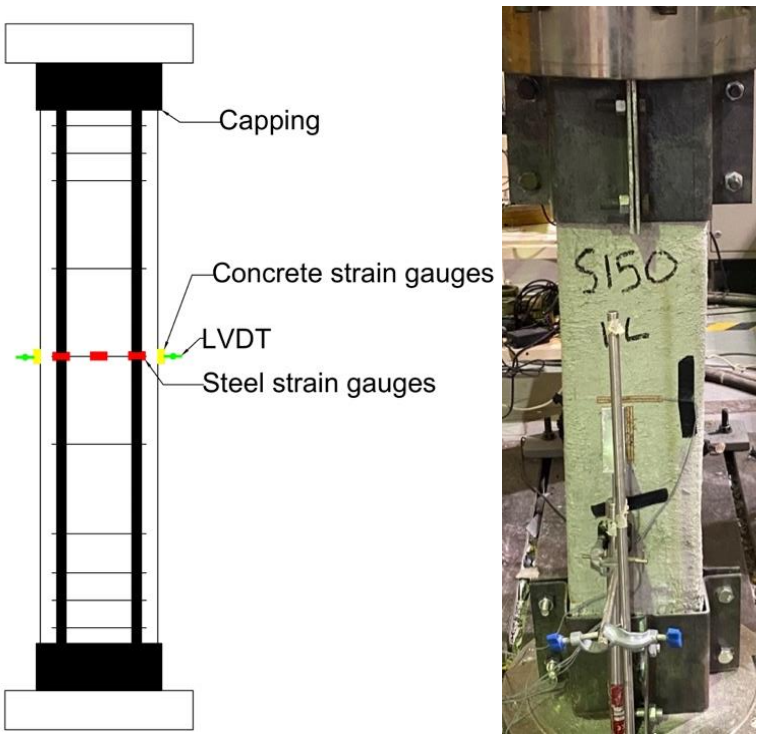

Figure 4: Pilot study specimen instrumentation.

3.2. Test Results and Discussion

Compressive test results are summarized in Table 5 where the column capacity, vertical displacement corresponding to the maximum load and failure mode are presented. All column failure modes are presented in Figure 5. Also, the ultimate capacity of square and circular columns was compared as shown in Figure 6.

Table 5: Pilot study test results.

Specimen	Maximum Load (kN)	Vertical Displacement (mm)	Failure Mode
Group 1: Square columns			
S0	722	7.1	Cracks and crushing near bottom grip; Diagonal crack; buckling in longitudinal reinforcement
S1	759	6.5	Bottom FRCM region; crack in cementitious matrix; fiber exposed
S2	821	10.2	Top FRCM region; crack in cementitious matrix; fiber exposed
S4	847	15.5	Mild damage near grips area
Group 2: Circular columns			
C0	687	2.1	Middle Region (close to the top grip); Diagonal crack
C1	682	5.0	Top FRCM region; crack in cementitious matrix; fiber exposed
C2	845	7.5	Bottom FRCM region; crack in cementitious matrix
C4	935	9.7	Mild damage near grips area

Results showed that a general increase in capacity for the columns strengthened with PBO-FRCM with the increase of number of layers. Square columns strengthened with PBO-FRCM showed a capacity increase of 5, 14 and 17% for 1 layer, 2 layers and 4 layers, respectively, while circular columns strengthened with PBO-FRCM showed a capacity increase of -1, 23 and 36% for 1 layer, 2 layers and 4 layers, respectively. Also, circular columns strengthened with 2 and 4 PBO-FRCM layers had a higher capacity than square columns by 3 and 10%, respectively. Premature failure at the regions of concentrated loading at the column ends was observed for some of the specimens. Furthermore, all columns showed an increase in ductility after

strengthening with PBO-FRCM as the displacement increased with the increase in number of PBO-FRCM layers, as shown in Table 5. Stress versus longitudinal reinforcement, vertical concrete and horizontal concrete strain relationships for all columns are shown in Figures 7, 8 and 9, respectively. Results showed that the variation of cross-section as well as the increase in number of PBO-FRCM layers had no effect on the stress-strain relationships for all columns.

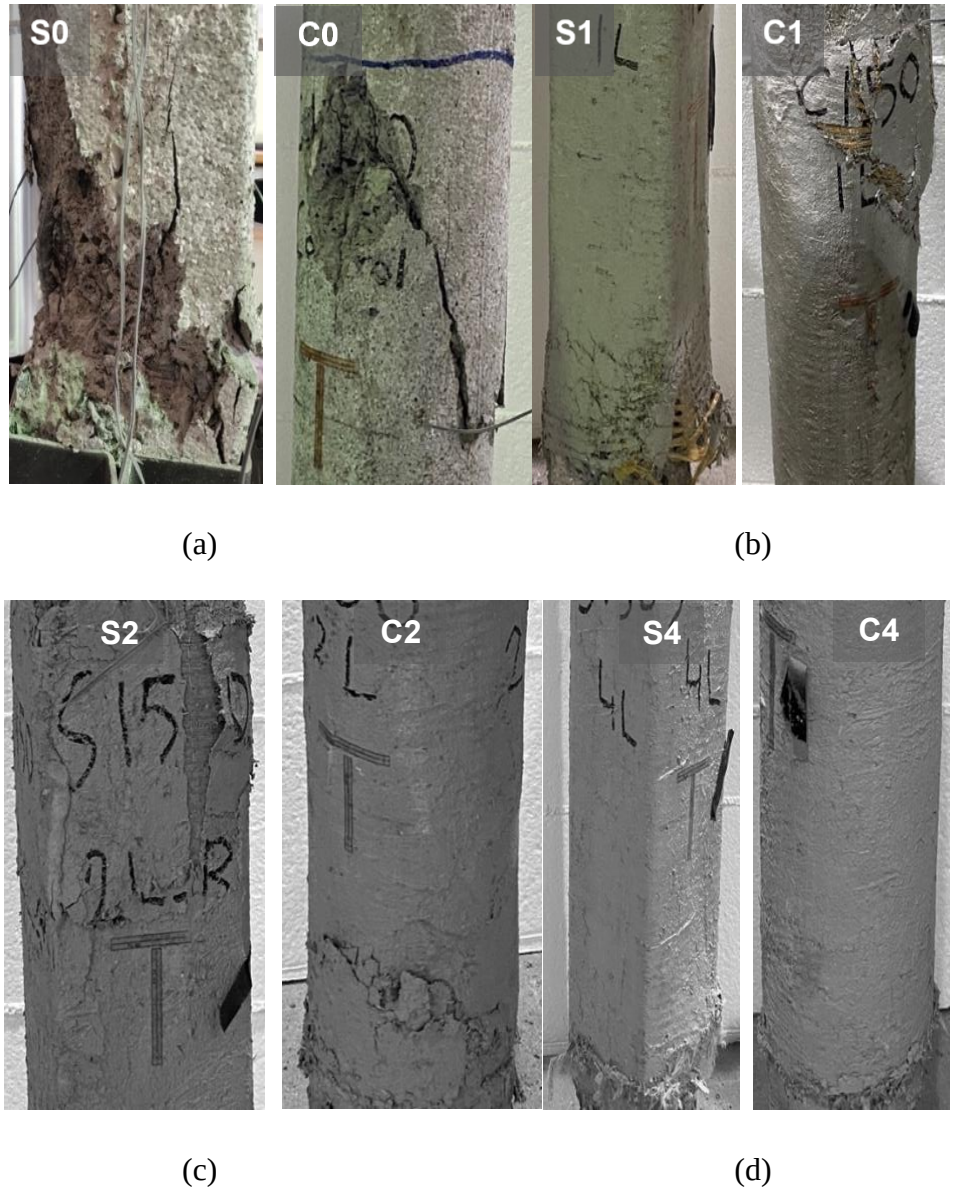

Figure 5: Pilot study failure modes of (a) control columns, (b) columns strengthened with 1 PBO-FRCM layer, (c) columns strengthened with 2 PBO-FRCM layers and (d) columns strengthened with 4 PBO-FRCM layers.

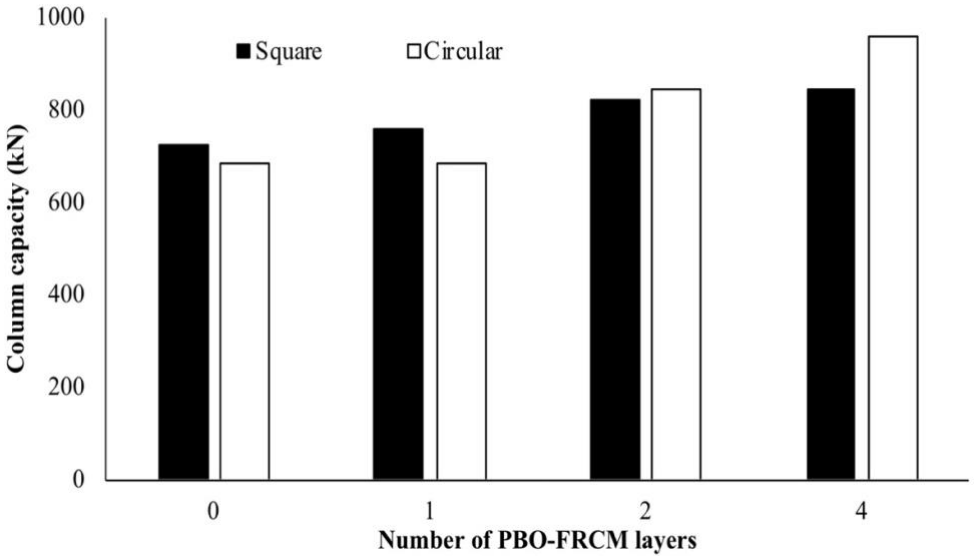

Figure 6: Comparison between the ultimate capacity of square and circular columns of the pilot study.

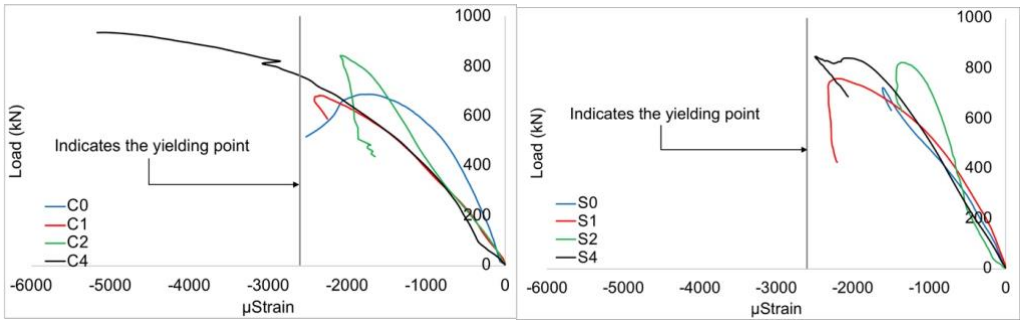

(a) (b)

Figure 7: Load versus longitudinal reinforcement strain of (a) square and (b) circular columns.

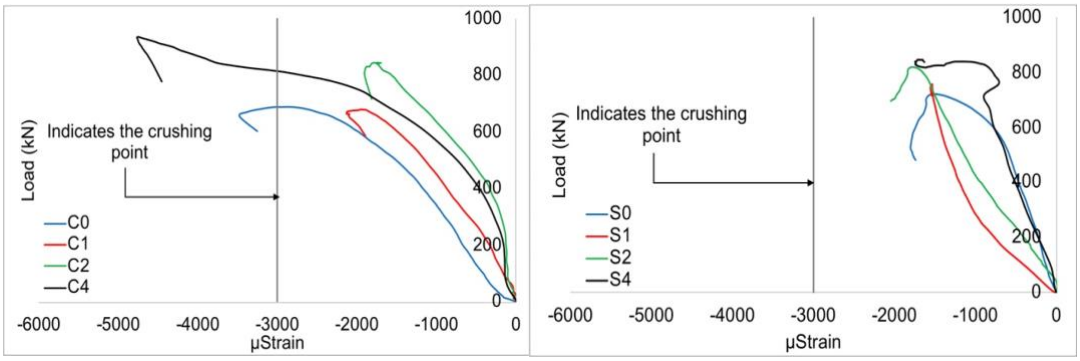

(a) (b)

Figure 8: Load versus vertical concrete/ FRCM strain of (a) square and (b) circular columns.

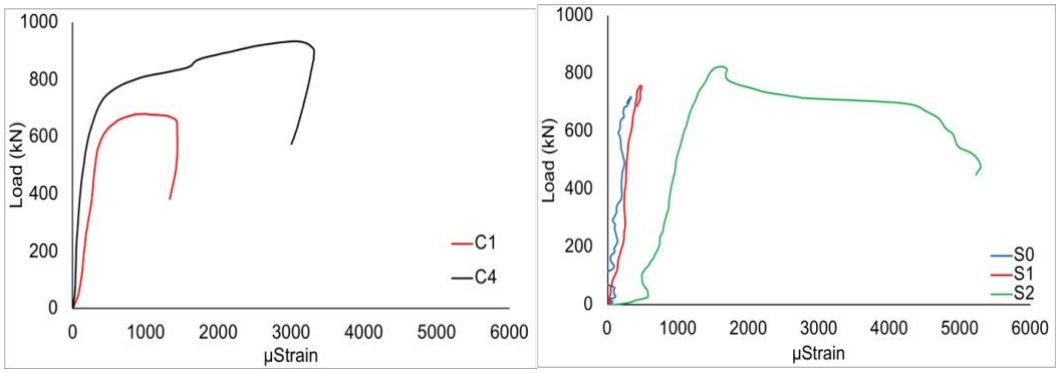

(a) (b)

Figure 9: Load versus horizontal concrete/ FRCM strain of (a) square and (b) circular columns.

3.3. Modifications Carried Forward for the Main Study

Fabrication of the pilot study's test specimens was modified based on the results and observed behavior of the pilot study's tested specimens in order to be used for the main study. A summary of the modifications applied on the fabrication of test specimens is presented in Table 6.

Table 6: Summary of test specimen fabrication modifications applied on the pilot study's specimens for the use in the main study.

Parameter		Pilot study	Main study
Pre-damaging		No	Yes
Cross-section dimensions (mm)	Square	150x150	180x180
	Circular	170	200
Concrete clear cover (mm)		15	20
Tie spacing (mm)		75	90
Longitudinal steel reinforcement ratio (%)	Square	2	1.4
	Circular	2	1.5
Prevention of local premature failure technique		Reducing the tie spacing at the column ends	Use of end corbels

Apart from subjecting the specimens in the main study to pre-damaging procedures prior to wrapping and testing, some parameters such as the column cross-

section, concrete clear cover and the number of PBO-FRCM layers used were modified. Also, the longitudinal steel reinforcement ratio was reduced in the main study due to the increase in column cross-sections while keeping the longitudinal reinforcement similar to the pilot study's specimens. Furthermore, the use of end corbels was introduced for the new specimens used in the main study in order to completely eliminate premature failure at column ends. Moreover, the tie spacing was increased to 90 mm for the main study.

Chapter 4. Experimental Program

In this chapter, the test matrix developed for this study as well as the design and fabrication procedure of the test specimens are thoroughly explained. Furthermore, the material properties of concrete, steel and PBO-FRCM used in this study are presented. Also, the procedure of wrapping the columns with PBO-FRCM followed by the test setup and instrumentation process are described in detail. Finally, the pre-damaging and reloading testing procedures are clarified.

4.1. Test Matrix

A total of 10 columns were cast for this study as shown in Table 7. The columns were divided into 2 main groups based on their cross-section. For each group, 1 column was unstrengthened, 2 columns were wrapped with 2 PBO-FRCM layers and 2 columns were wrapped with 4 PBO-FRCM layers. The unstrengthened column within each group was loaded up to failure and served as the control specimen. For the columns wrapped with PBO-FRCM layers, 2 columns were wrapped and loaded up to failure, while the other 2 columns were pre-damaged up to ultimate load, unloaded, wrapped, then reloaded up to failure. The specimen numbering system consisted of an initial letter indicating the type of cross-section, where S indicated square columns and C indicated circular columns. The initial letter was followed by a dash and a number indicating the number of PBO-FRCM layers, where 0 indicated unstrengthened columns, 2 indicated columns strengthened with 2 PBO-FRCM layers and 4 indicated columns strengthened with 4 PBO-FRCM layers. Then, the number indicating the number of PBO-FRCM layers was followed by a dash and the pre-damaging condition, where Control indicated that the column was served as control without any pre-damage, ND indicated that the column was not pre-damaged, and PD indicated that the column was pre-damaged up to ultimate load.

4.2. Design of Test Specimens

The fabrication of columns for this study was based on the pilot study mentioned in the previous chapter and its results. All columns were designed to behave as short columns to ensure the pure subjection to axial loading and to prevent inducing moment due to eccentricity. To ensure the aforementioned behavior, the columns were designed according to ACI 318-19 provisions [48] using Equations 1 and 2 given by:

$$\frac{kl_u}{r} > 22 \quad (1)$$

$$r = \frac{I_g}{A_g} \quad (2)$$

where k is the effective length factor, l_u is the column height, r is the radius of gyration, I_g is the gross inertia and A_g is the cross-sectional area of the column.

The column dimensions for both square and circular cross-sections were increased from the dimensions in the pilot study, in order to accommodate the need of increasing the concrete clear cover after facing some problems with concrete casting of the specimens in the pilot study. The side dimension of the square columns was increased to 180 mm and the diameter of the circular columns was increased to 200 mm. The concrete clear cover was increased to 20 mm for both types of cross-section. Longitudinal reinforcement for both square and circular columns was kept the same as in the pilot study, where square columns were reinforced with 4 bars of 12 mm diameter and the circular columns were reinforced with 6 bars of 10 mm diameter. Bars were disturbed uniformly for both types of cross-section. Since the cross-sectional area was increased and the longitudinal reinforcement area remained the same as in the pilot study, the reinforcement ratio decreased to 1.4 and 1.5% for the square and circular columns, respectively. Figure 10 shows the longitudinal cross-sections of square and circular columns. Figure 11 shows the square and circular cross-sections used in this study. To calculate the theoretical ultimate capacity of the columns according to the new dimensions, Equation 3 from the ACI 318-19 code [48] was used:

$$P_n = A_s f_y + 0.85 f'_c (A_g - A_s) \quad (3)$$

where A_s is the area of longitudinal steel reinforcement, f_y is the tensile yield strength of steel bars and f'_c is the specified compressive strength of concrete.

All columns were transversely reinforced with 6 mm ties spaced at 90 mm. To enhance the prevention of premature failure and ensure that failure occurs within the columns and not due to concentrated loading at the column ends, 400 x 400 mm square corbels were cast at both ends of all columns. The end corbels had a height of 200 mm and were reinforced with longitudinal bars of 10 mm diameter and ties of 8 mm and 10 mm diameters as shown in Figure 12. All columns had a clear height of 800 mm.

Table 7: Test matrix.

Specimen	Reinforcement	Reinforcement ratio (%)	FRCM layers
Group A: Square columns			
S-0-Control	4ϕ12	1.4	-
S-2-ND	4ϕ12	1.4	2
S-2-PD	4ϕ12	1.4	2
S-4-ND	4ϕ12	1.4	4
S-4-PD	4ϕ12	1.4	4
Group B: Circular columns			
C-0-Control	6ϕ10	1.5	-
C-2-ND	6ϕ10	1.5	2
C-2-PD	6ϕ10	1.5	2
C-4-ND	6ϕ10	1.5	4
C-4-PD	6ϕ10	1.5	4

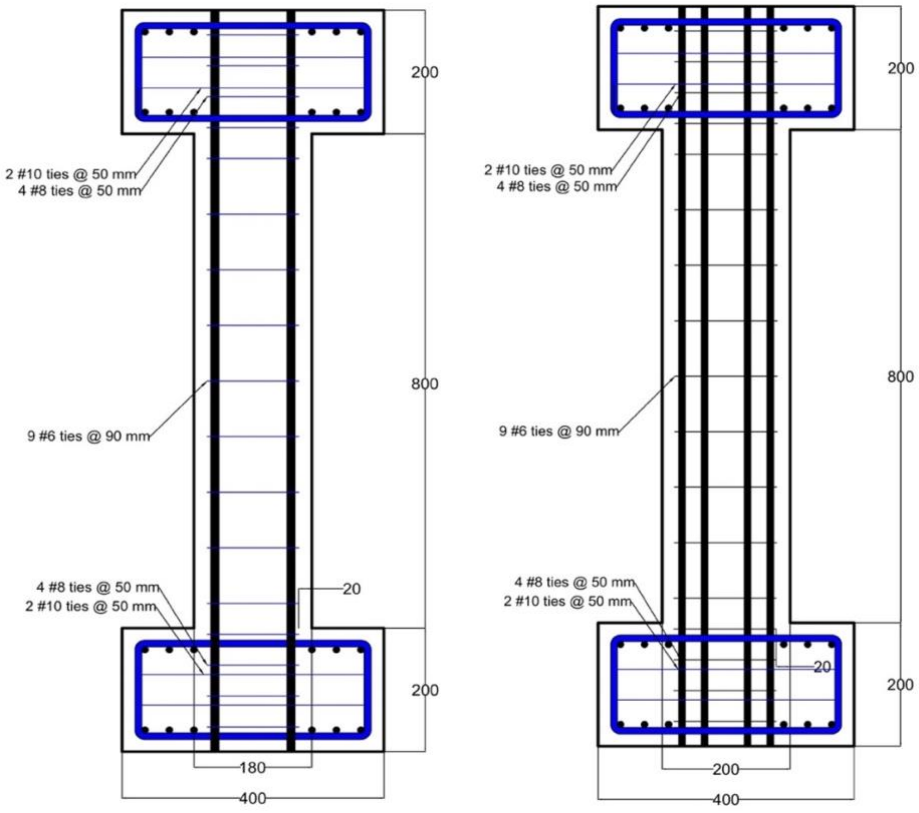

(a) (b)

Figure 10: Longitudinal cross-section of (a) Group A and (b) Group B columns.

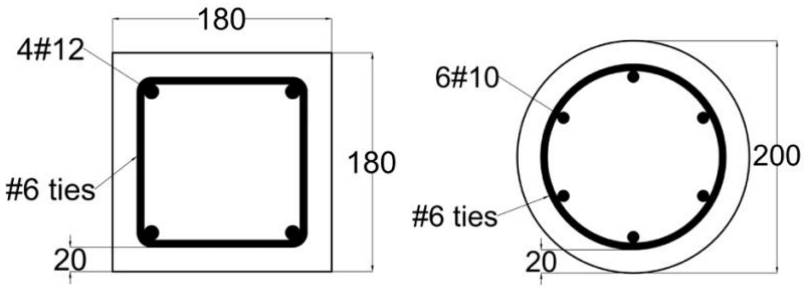

(a) (b)

Figure 11: Cross-section of (a) square and (b) circular columns.

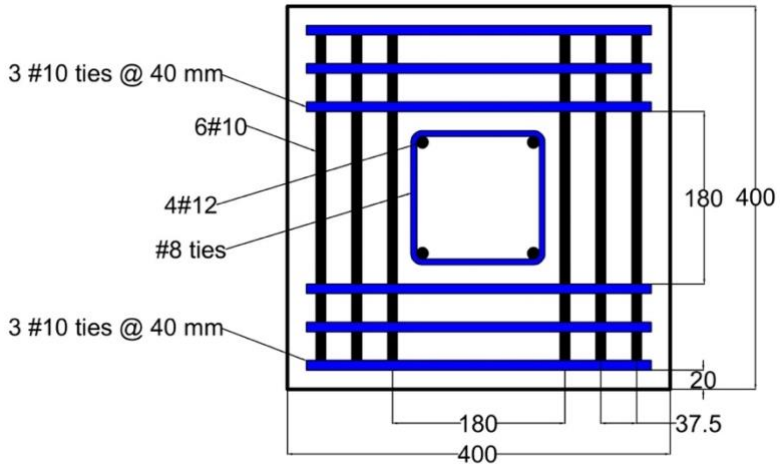

(a)

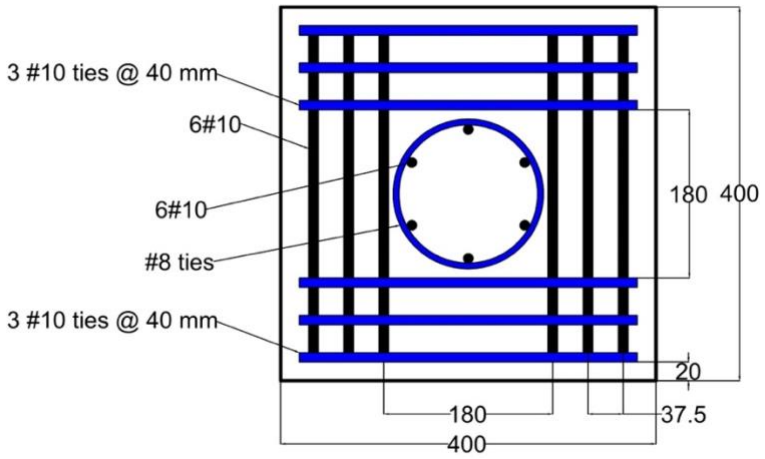

(b)

Figure 12: End corbels cross-section of (a) square and (b) circular columns.

4.3. Material Properties

4.3.1. Steel. In this study, square columns were longitudinally reinforced with 4 equally spaced ribbed steel bard of 12 mm diameter. Circular columns were longitudinally reinforced with 6 equally spaced ribbed steel bard of 10 mm diameter. All columns were transversely reinforced with steel ties of 6 mm diameter. In order to obtain the yield and tensile strength of the rebars and ties, tensile tests were conducted on samples of the steel bars in accordance with ASTM A370 provisions [51]. Results showed that the yield and tensile strengths of the longitudinal reinforcing bars were 490 MPa and 610 MPa, respectively. The yielding strain for the longitudinal reinforcing bars was 0.0026. Figure 13 shows the tensile strength test results for 3 bar samples of diameter 10 mm and 12 mm. The yield and tensile strengths of the ties were 280 MPa and 300 MPa, respectively. The steel cages were prepared before casting as shown in Figure 14.

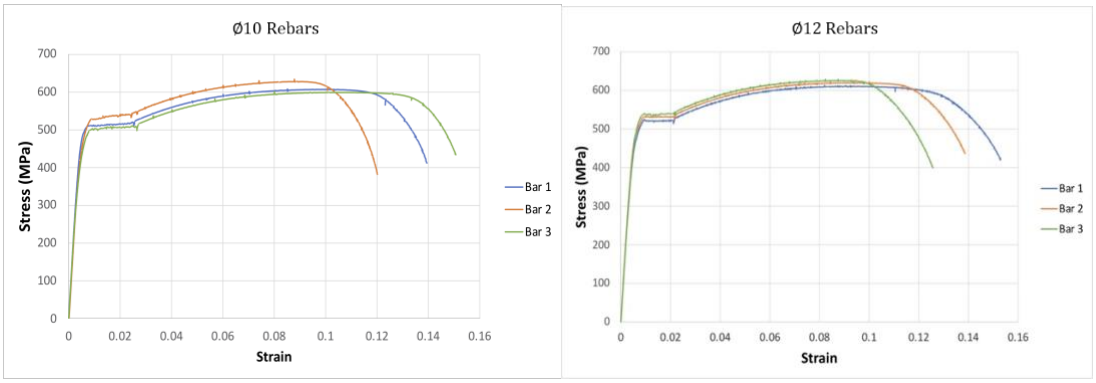

(a) (b)

Figure 13: Stress versus strain for rebar samples of size (a) 10 mm and (b) 12 mm.

4.3.2. Concrete. All columns were cast at Emirates Stone Company in Sharjah, UAE. 5 standard 150 x 300 mm cylinders were cast along with the columns. All cylinders were tested on the day of column testing according to ASTM C39 [37] where the results are tabulated in Table 8. Cylinders had an average compressive strength of 20 MPa. The formwork that was used for casting is shown in Figure 15. Cast columns are shown in Figure 16.

(a) (b)

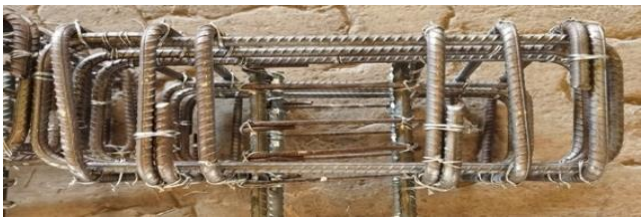

(c)

Figure 14: (a) Square columns, (b) circular columns and (c) end corbels steel cages.

Table 8: Cylinders compressive strength.

Cylinder	Compressive strength (MPa)	Average compressive strength (MPa)
1	20.76	
2	20.71	
3	20.77	20.03
4	18.85	
5	19.08	

(a) (b)

Figure 15: Formwork used to cast (a) square and (b) circular columns.

Figure 16: Cast specimens.

4.3.3. PBO-FRCM. The PBO-FRCM used for strengthening in this study was provided by RureGold Company, where PBO-MESH GOLD 70/18 and PBO-MESH GOLD CALCESTRUZZO were supplied. PBO-MESH GOLD 70/18 is a bidirectional PBO fiber mesh with 70 g/m^2 in wrap and 18 g/m^2 in weft. It has a tensile strength of 5.8 GPa, an elastic modulus of 270 GPa, a fiber density of 1.56 g/cm^3 and an elongation at rupture of 2.5%. The mesh was supplied along with PBO-MESH GOLD CALCESTRUZZO, which was the stabilized inorganic matrix used to bind the mesh to

the concrete surface. A sample of the mesh is shown in Figure 17. The properties of the bidirectional mesh and the inorganic matrix are tabulated in Tables 9 and 10, respectively.

Figure 17: Sample of PBO-FRCM provided by RureGold.

Table 9: Properties of the PBO-FRCM bidirectional mesh according to the manufacturer's datasheet.

Properties of the Bidirectional Mesh	**PBO-MESH GOLD 70/18**
Weight of PBO fibers in the mesh	88 g/m^2
Equivalent thickness of dry fabric in the direction of the wrap	0.0455 mm
Equivalent thickness of dry fabric in the direction of the weft	0.0115 mm
Tensile strength of the wrap per unit of length	264.0 kN/m
Tensile strength of the weft per unit of length	66.5 kN/m
Weight of the mesh (support + PBO fibers)	110 g/m^2

Table 10: Properties of the PBO-FRCM inorganic matrix according to the manufacturer's datasheet.

Properties of the Inorganic Matrix	**PBO-MESH GOLD CALCESTRUZZO**
Water per 100 kg of dry premix	26-28 liters
Consistency of the mortar (EN13395-1)	175 +/- 10 mm
Specific weight of fresh mortar (EN 1015-6)	1.80 ± 0.05 g/cc
Volume of fresh mortar for 100 kg of dry premix	About 71 liters
Compression resistance at 28 days (EN12190)	≥ 40 MPa
Bending resistance at 28 days (EN 196-1)	≥ 4 MPa
Elastic modulus at 28 days (EN 13412)	≥ 7 GPa

4.4. Pre-Damaging Stage

As previously mentioned in the test matrix (section 4.1), columns S-2-PD, S-4-PD, C-2-PD and C-4-PD were subjected to pre-damaging procedures prior to PBO-FRCM wrapping and reloading up to failure. The motivation behind subjecting those columns to pre-damaging was to help simulate existing deteriorated columns that need rehabilitation. The pre-damaging procedure was similar to that of reloading that is explained later in section 4.6, where columns were tested monotonically using a Universal Testing Machine (UTM) under a loading rate of 0.3 mm/min. The test was manually halted right upon reaching ultimate load, which was previously determined from testing the control columns S-0-Control and C-0-Control up to failure. Prior to initiating the tests, LVDT's were installed at mid height of the columns to measure the axial displacement. Strain gauges were also mounted on the main longitudinal rebar to measure the strain in those bars throughout the tests. All LVDT's and strain gauges were connected to a digital data acquisition system that records data at a rate of 600 readings/min. Figure 18 shows all the pre-damaged columns after unloading. Figure 19 shows the graphs of load versus strain in longitudinal steel bars of pre-damaged columns during pre-damaging stage. As clearly indicated in the figure, the steel reinforcement of all pre-damaged columns reached the yielding strain of 0.0026 before unloading.

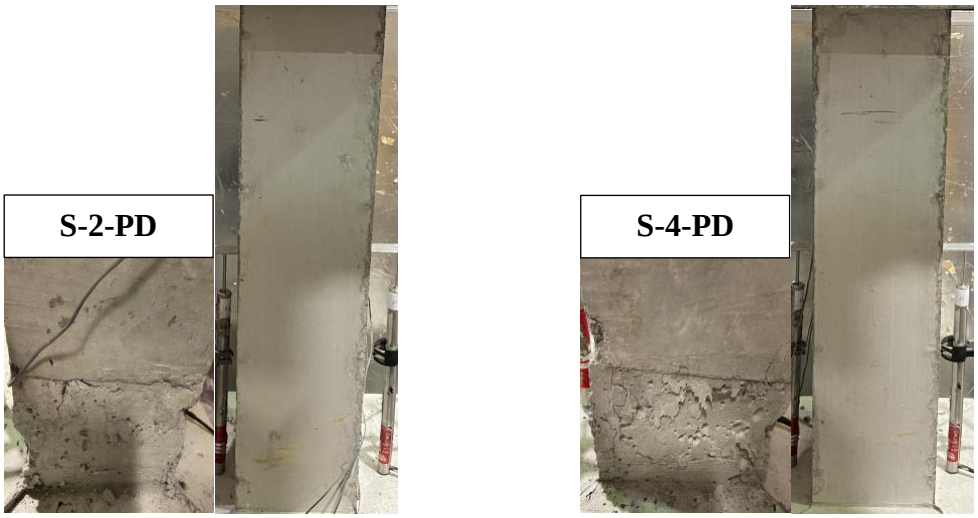

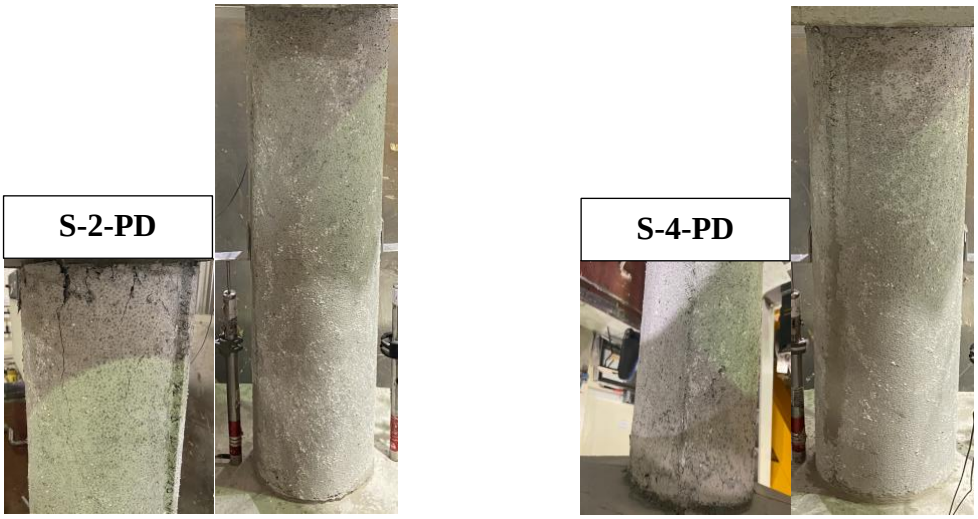

Figure 18: Pre-damaged columns after unloading.

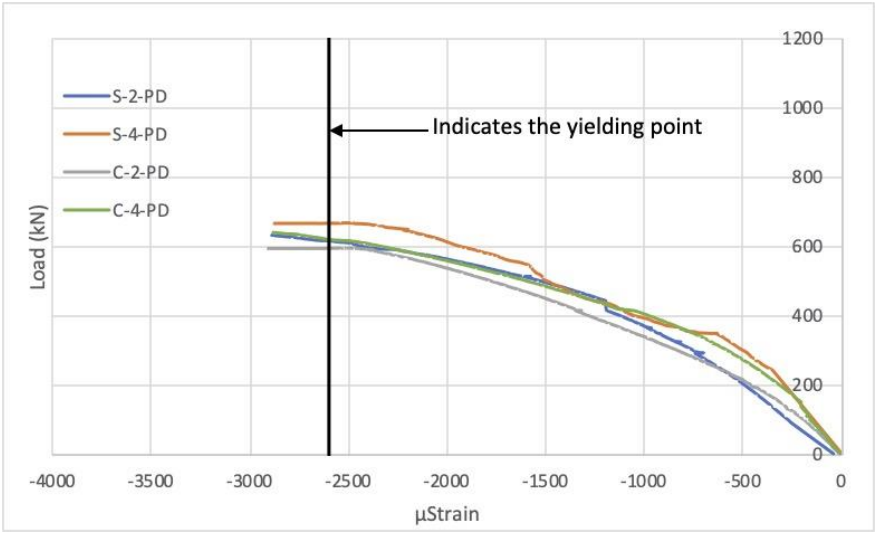

Figure 19: Load versus strain for pre-damaged columns during pre-damaging.

4.5. PBO-FRCM Installation

As shown in the test matrix in Table 7, 1 column of each group was not strengthened and served as control, 2 columns were wrapped then loaded up to failure, and 2 columns were pre-damaged, unloaded, wrapped, then reloaded up to failure. For all strengthened columns, the PBO-FRCM installation procedure was executed as follows:

4.5.1. Surface preparation. Before wrapping, the surface had to be prepared properly. For square cross-section, the corners were grinded using a grinder until smooth as shown in Figure 20. Furthermore, the surface of the specimens was roughened either by using a grinder and a steel brush until the surface was rough enough for mortar to stick on it. After that, specimens were cleaned to remove, and dust remaining on the surface and then were sprayed with water to ensure the concrete would not absorb the water from the mortar after it got applied.

(a) (b)

Figure 20: Square columns edges (a) during grinding and (b) after grinding.

4.5.2. Mortar and mesh preparation. Each bag of cementitious mix weighing 25 kg was mixed with 6.3 L of water, as per the supplier's recommendation. An electric drill with a speed of less than 500 rpm was used to mix the cementitious mix to ensure that the polymers were distributed evenly and were mixed well. A bucket was used to do the mixing where 80% of the water was put first, then the powder was added gradually while mixing as shown in Figure 21. After that, the remaining 20% of

water was added gradually. Before wrapping, the mesh was cut and prepared according to the needed dimensions with an additional overlap length of 100 mm as shown in Figure 22.

(a) (b)

Figure 21: Mortar mixing process.

Figure 22: Mesh preparation process.

4.5.3. Wrapping. Figure 23 illustrates the wrapping process. The first step of the wrapping procedure was to wet the concrete surface of the specimens using a brush. After that, a 4 mm mortar layer was applied manually on the concrete surface and smoothed using a trowel while spraying with water simultaneously. Then, a mesh layer

was applied by pressing it on top of the mortar while ensuring it was as impregnated as possible with no gaps. A second layer of mortar was applied on top of the mesh. For columns wrapped with 2 PBO-FRCM layers, a second layer of mesh was applied following the same aforementioned procedure followed by a last layer of mortar. The same procedure was followed for the columns wrapped with 4 PBO-FRCM layers until the total of installed layers was 4, where the last layer had to be mortar. At the end, the wrapped specimens were sprayed with water and smoothed using a trowel. All wrapped specimens were cured for 10 days before testing with wet burlap as shown in Figure 23(g).

(a) (b) (c)

(d) (e) (f)

(g)

Figure 23: PBO-FRCM installation process.

4.6. Test Setup and Instrumentation

Prior to casting, strain gauges were installed at the midpoint of 2 steel bars opposing each other for each steel cage as shown in Figure 24. Also, a strain gauge was installed on the middle tie of each steel cage. After casting, curing for 28 days, pre-damaging for specimens that were scheduled to get subjected to damaging, wrapping with PBO-FRCM for specimens that had to be strengthened, additional horizontal and vertical strain gauges were installed at the midpoint of the column surface. After mounting each specimen on the testing machine, 2 LVDT's were vertically mounted on opposite sides of the column in order to measure the vertical displacement. All strain gauges and LVDT's were connected to a digital data acquisition system that records data at a rate of 600 readings/min. All columns were tested using a UTM at the American University of Sharjah at a rate of 0.3 mm/min. The maximum capacity of the UTM was 2500 kN. Columns were mounted on the machine in a manner where their longitudinal axes coincided with the line of action of the exerted force. Figure 25 shows the test setup schematics and a typical specimen setup on the UTM machine.

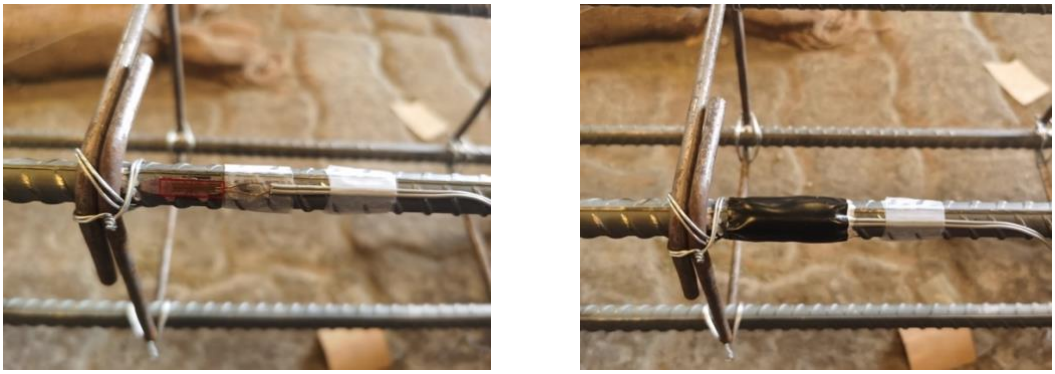

(a) (b)

Figure 24: Strain gauge installation on rebars.

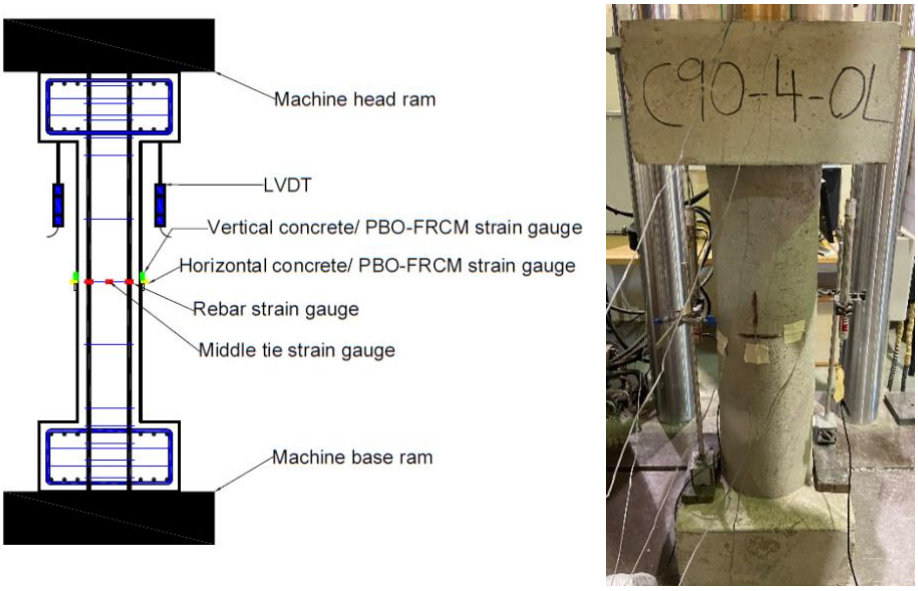

Figure 25: Test setup and instrumentation schematics.

Chapter 5. Experimental Results

In this chapter, all experimental results are presented. The ultimate capacities, axial displacements, load-strain relationships, and failure modes for all tested specimens are exhibited.

5.1. Axial Capacity

Table 11 shows a summary of the experimental results where the pre-damaging maximum load, ultimate capacity, percentage of increase in ultimate capacity, axial displacement at ultimate capacity and ductility are presented. The increase in ultimate capacity of each column was calculated with respect to the unwrapped control specimen of the group the column belonged to. For example, the capacity increase percentage for columns S-2-ND, S-2-PD, S-4-ND and S-4-PD was calculated with respect to the ultimate capacity of column S-0-Control. LVDT's were used to record the vertical displacement of all columns corresponding to the increasing load during the compressive tests. Figures 26 and 27 show the load versus displacement graphs for all tested columns. Furthermore, column ductility was calculated by dividing the displacement at 80% of the ultimate load reached after unloading divided by the axial displacement at yielding as shown in Equation 4, which is an approximate method proposed by Shannag et al. [52].

Table 11: Summary of experimental results.

Specimen	Pre-damaging max load (kN)	Ultimate capacity (kN)	Increase in ultimate capacity (%)	Displacement at ultimate capacity (mm)	Ductility
S-0-Control	-	660.1	-	2.2	4.5
S-2-ND	-	796.7	20.7	5.3	5.4
S-2-PD	659.8	795.2	20.5	4.1	5.4
S-4-ND	-	891.7	35.1	12.9	6.8
S-4-PD	668.9	935.8	41.8	5.5	6.2
C-0-Control	-	615.2	-	1.8	4.3
C-2-ND	-	862.5	40.2	10.1	5.6
C-2-PD	596.5	852.0	38.5	8.3	5.7
C-4-ND	-	1035.8	68.4	15.9	7.7
C-4-PD	661.7	1053.7	71.3	14.9	7.7

$$DD = \frac{\delta_m}{\delta_y} \quad (4)$$

where DD is the displacement ductility, δ_m is the displacement at 80% of the ultimate load reached after unloading and δ_y is the displacement at yield load.

5.2. Axial load versus Displacement

The load versus displacement behavior of all control columns (S-0-Control and C-0-Control) was similar before reaching peak load, where the response can be divided into 3 stages. The initial stage consists of a linearly ascending branch, followed by a semi-linearly ascending branch with a gradual decrease in stiffness up till peak load. The third stage consisted of a gradual drop in load. The first stage stiffness for all unwrapped control columns ranged between 462-658 kN/mm.

All wrapped columns that were not pre-damaged (S-2-ND, S-4-ND, C-2-ND and C-4-ND) displayed a pre peak load behavior similar to the unwrapped control columns, where the initial stiffness was lower than the unwrapped control columns ranging between 202-300 kN/mm. After reaching peak load, wrapped columns displayed a gradual descending behavior, where all columns wrapped with 4 PBO-FRCM layers had multiple peak load points after the first one. It was evident that wrapping columns with PBO-FRCM significantly increased the ductility due to the increase in the displacement range after reaching peak load, where the increase was higher for columns wrapped with 4 layers.

Furthermore, all pre-damaged columns strengthened with PBO-FRCM (S-2-PD, S-4-PD, C-2-PD and C-4-PD) had a similar behavior in the pre-damaging phase, as indicated in Figures 26(b) and 27(b), where the curve could be divided into three stages. The first stage consists of a linearly ascending branch followed by a semi-linearly ascending branch with a gradual decrease in stiffness up to peak load. After reaching peak load, the curve showed similar stiffness to the initial stiffness while the column was being unloaded. After wrapping columns with PBO-FRCM and reloading up to failure, the columns showed similar initial stiffness to the one demonstrated during the pre-damaging phase. All pre-damaged wrapped columns showed higher ductility than the unwrapped ones with the increase being higher for columns wrapped with 4 PBO-FRCM layers.

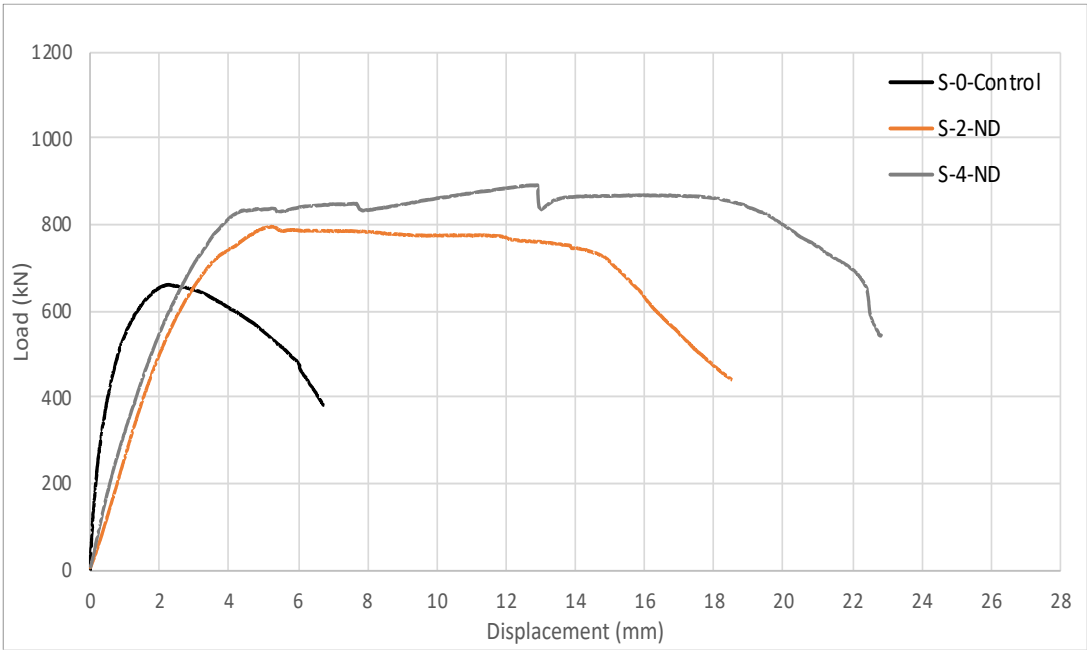

(a)

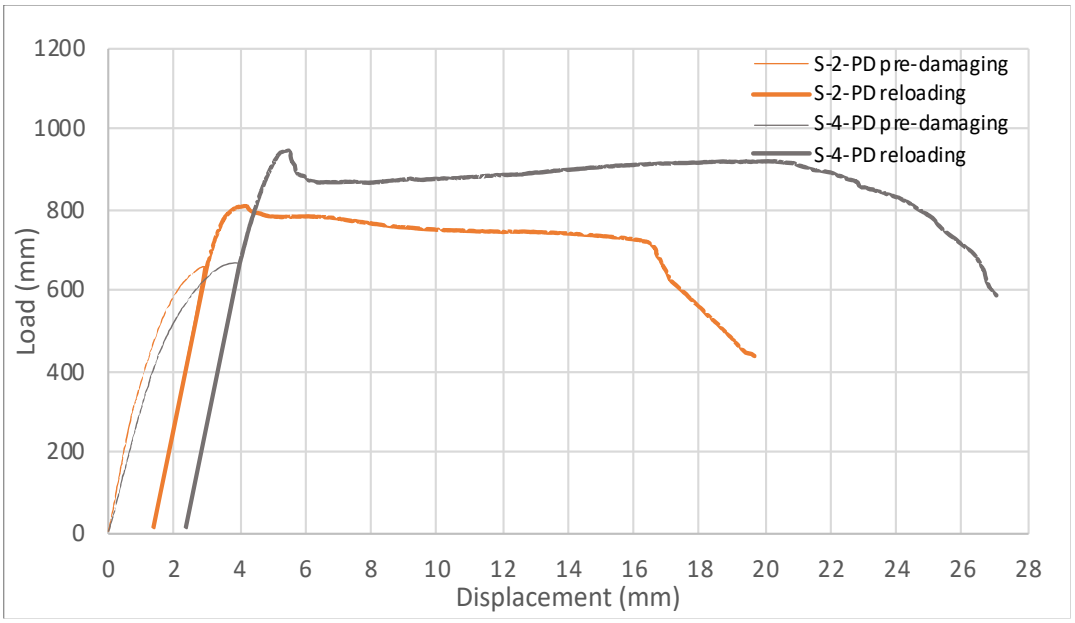

(b)

Figure 26: Load versus displacement for (a) control and (b) pre-damaged columns in Group A.

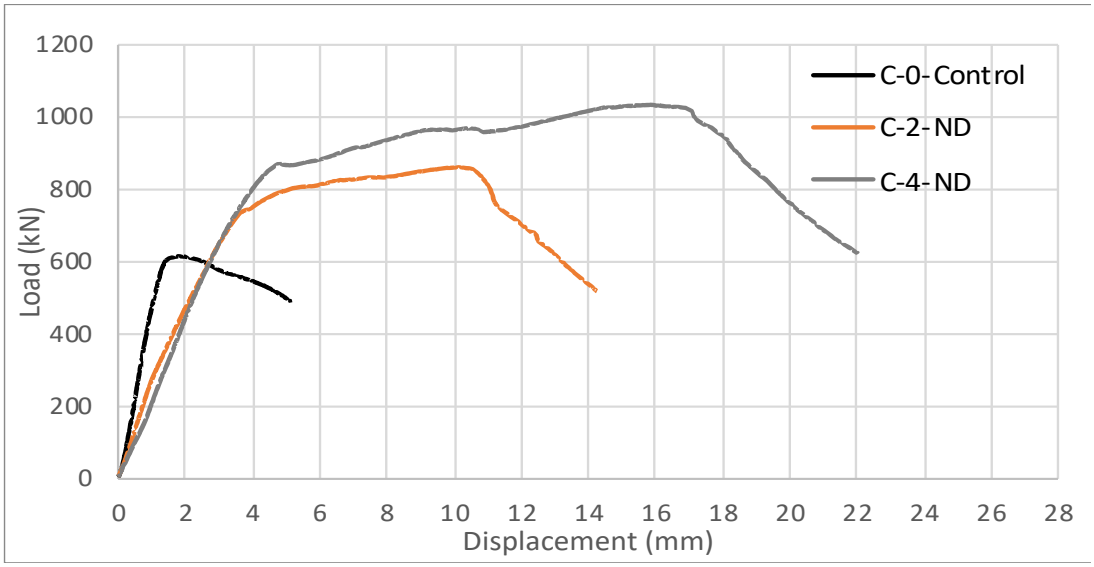

(a)

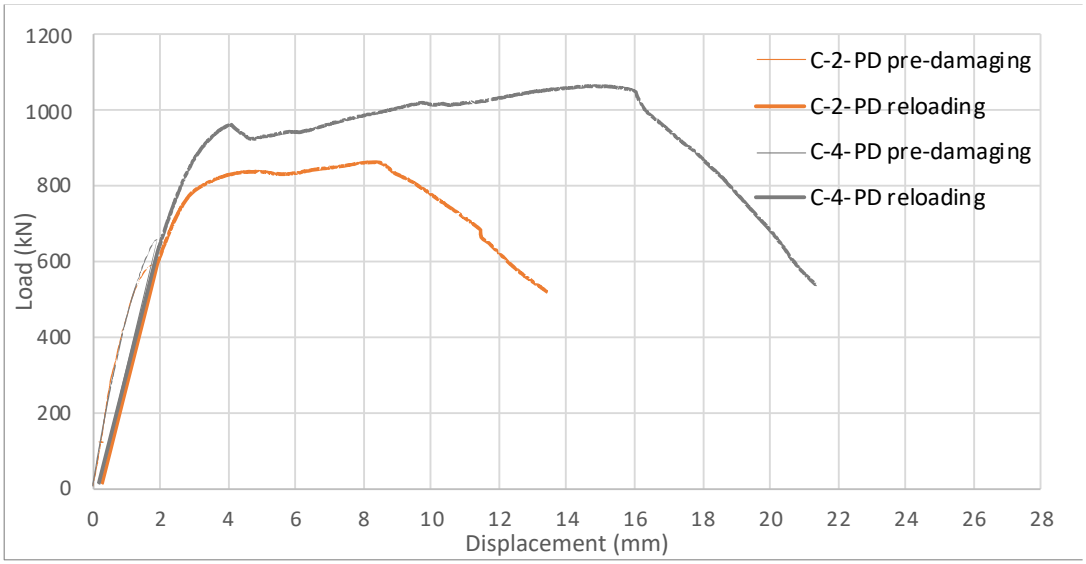

(b)

Figure 27: Load versus displacement for (a) control and (b) pre-damaged columns in Group B.

5.3. Load-Strain Relationships

The load versus strain relationships in steel longitudinal bars, middle ties, longitudinal concrete, and transverse concrete are presented in this section.

5.3.1. Load versus longitudinal steel strain. Prior to concrete casting, strain gauges were installed at the middle of 2 of the steel longitudinal reinforcing bars, as well as the middle tie. The readings of the average of the steel rebars strain versus axial

load for all columns in the reloading phase are displayed in Figure 28. The curve consisted of a linearly ascending branch followed by a semi-linearly ascending branch with a gradual decrease in stiffness up till peak load. After reaching peak load, columns showed one of two main behaviors. The first one was maintaining a constant strain value until the point where the test was halted, whereas the second one was showing a sharp drop in load. For columns in Group A, all columns showed the first kind of behavior after reaching peak load except for column S-4-PD, which showed an instantaneous sudden drop in load followed by maintaining a constant strain until the test was halted. Also, all Group A column rebars reached the yielding capacity. For Group B, columns C-2-ND, C-2-PD and C-4-PD showed the first kind of behavior post peak load while columns C-0-Control and C-4-ND showed the second kind of behavior. All wrapped columns rebars reached yielding capacity, while the control column rebars did not.

5.3.2. Load versus middle tie strain. Load versus middle tie strain behavior of tested columns is shown in Figure 29. The load versus middle tie strain graphs of columns S-2-ND and S-4-PD are missing due to damage in the strain gauges connected to the middle ties during concrete casting or the pre-damaging procedures. Strain in all middle ties reached very low levels, as strain did not exceed 500 μStrain for most columns. Furthermore, the middle tie strain behavior was similar for all columns except for column S-4-ND, and it consisted of 2 main stages. The first stage consisted of a linearly ascending branch, followed by a sharp drop in load when the test was halted. Middle tie strain of column S-4-ND showed a slightly different behavior where the curve consisted of 3 stages rather than 2. Similar to the rest of the columns, the first stage consisted of a linearly ascending branch. Then, the curve showed a semi-linearly ascending behavior with a gradual decrease in stiffness. After reaching peak load, the curve flattened until the test was halted.

5.3.3. Load versus longitudinal concrete strain. The load versus longitudinal concrete strain graphs for all columns are shown in Figure 30. For all control columns, strain gauges were installed vertically at the mid-height of the concrete surface in order to obtain the longitudinal concrete strain readings during the reloading phase of the test. For all non-damaged wrapped columns and columns that got wrapped after the pre-damaging procedures, strain gauges were also vertically installed at mid-

height of the outer surface of FRCM to obtain the strain readings during the tests. All columns showed similar longitudinal concrete strain behavior where the curve initiated with a linearly ascending branch, followed by a semi-linearly ascending branch with a gradual decrease in stiffness up till peak load. After reaching peak load, curves displayed a drop in load. None of the strain gauges indicated concrete reaching the concrete crushing strain of 3000 µStrain except for column C-2-PD.

5.3.4. Load versus transverse concrete strain. The load versus transverse concrete strain graphs for all columns are shown in Figure 31. Horizontal concrete strain gauges were installed on the columns along with the vertical concrete ones. All square columns exhibited similar transverse concrete strain behavior, where the curves could be divided into 3 sections. The first section consisted of a linearly ascending branch up till peak load. After reaching peak load, an instantaneous drop in load could be noticed, followed by flattening of the curve until the point where the test was halted. The post peak curve plateau indicates an increase in the the lateral deformation due to the FRCM confinement which in turn enhances the ductility of the column at a sustained loading capacity. For circular columns, the initial linear curve behavior up till peak load was similar to that of the square columns. However, not all circular columns showed curve flattening after peak load. For Group B, all wrapped columns showed flattening post peak load.

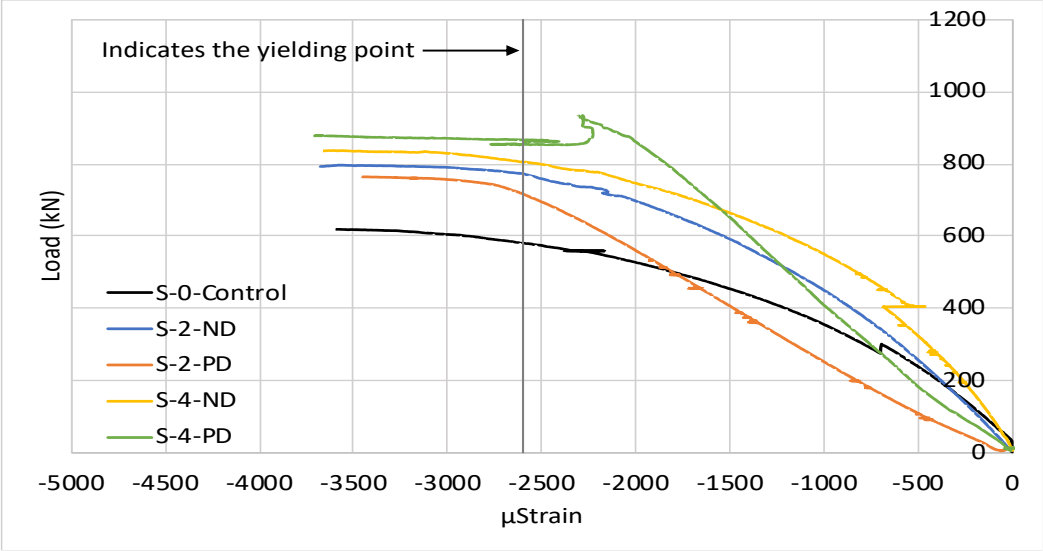

(a)

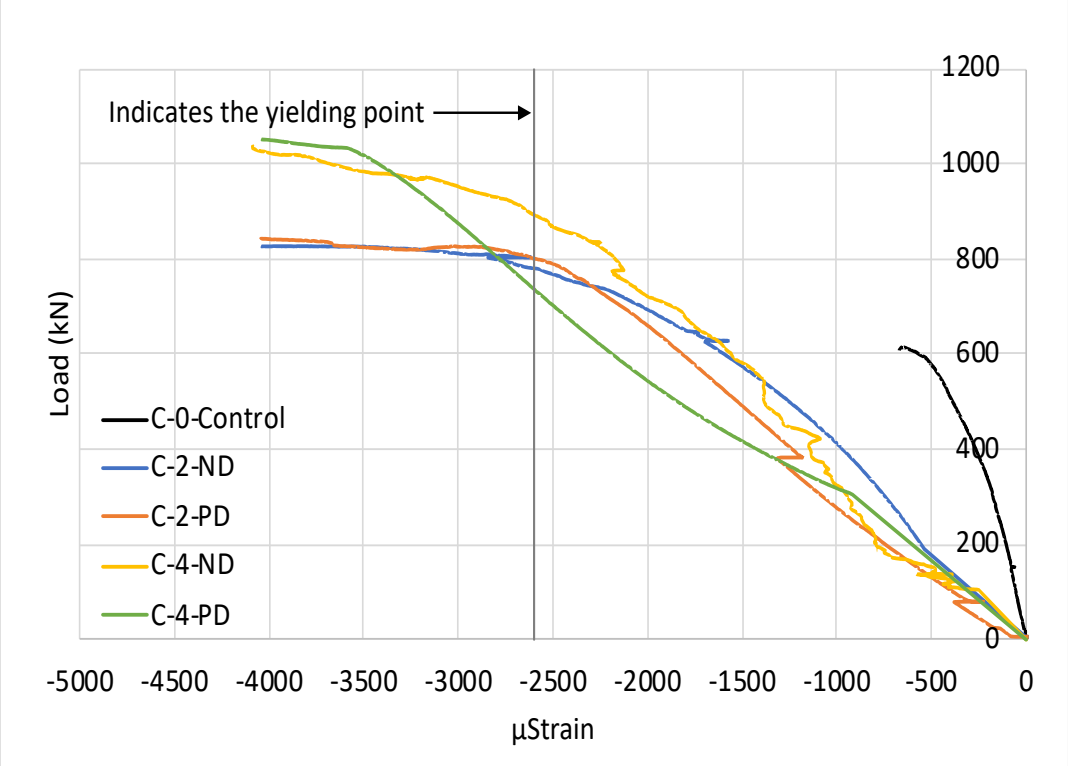

(b)

Figure 28: Load versus reinforcement bar strain for (a) Group A and (b) Group B.

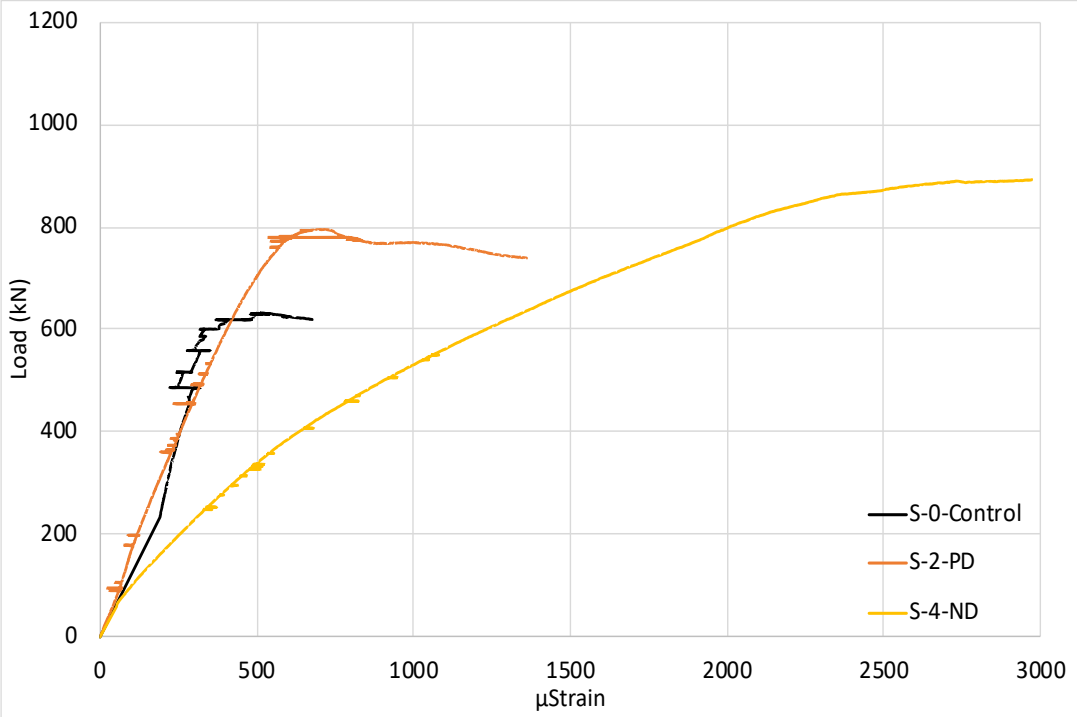

(a)

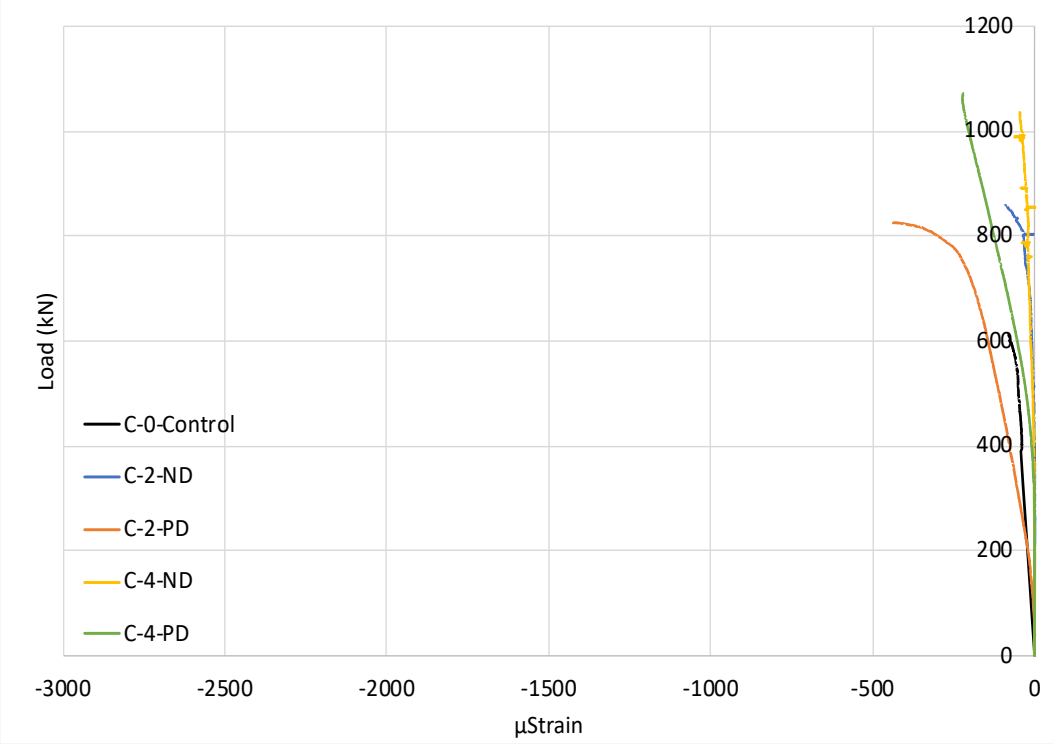

(b)

Figure 29: Load versus middle tie strain for (a) Group A and (b) Group B.

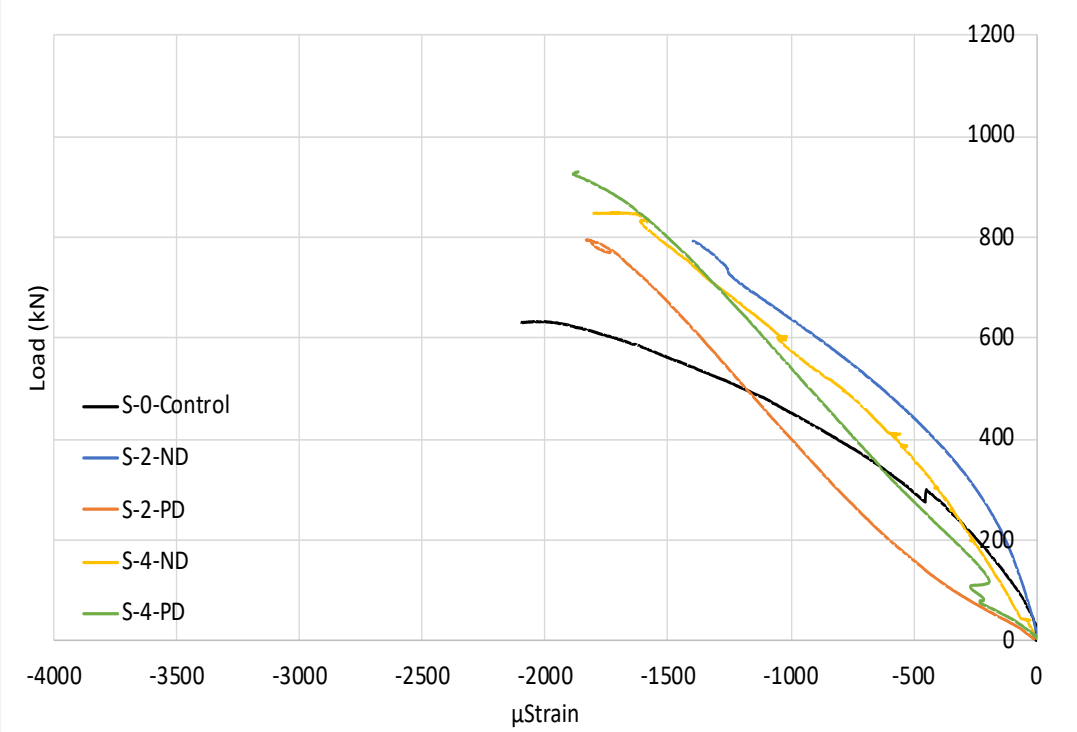

(a)

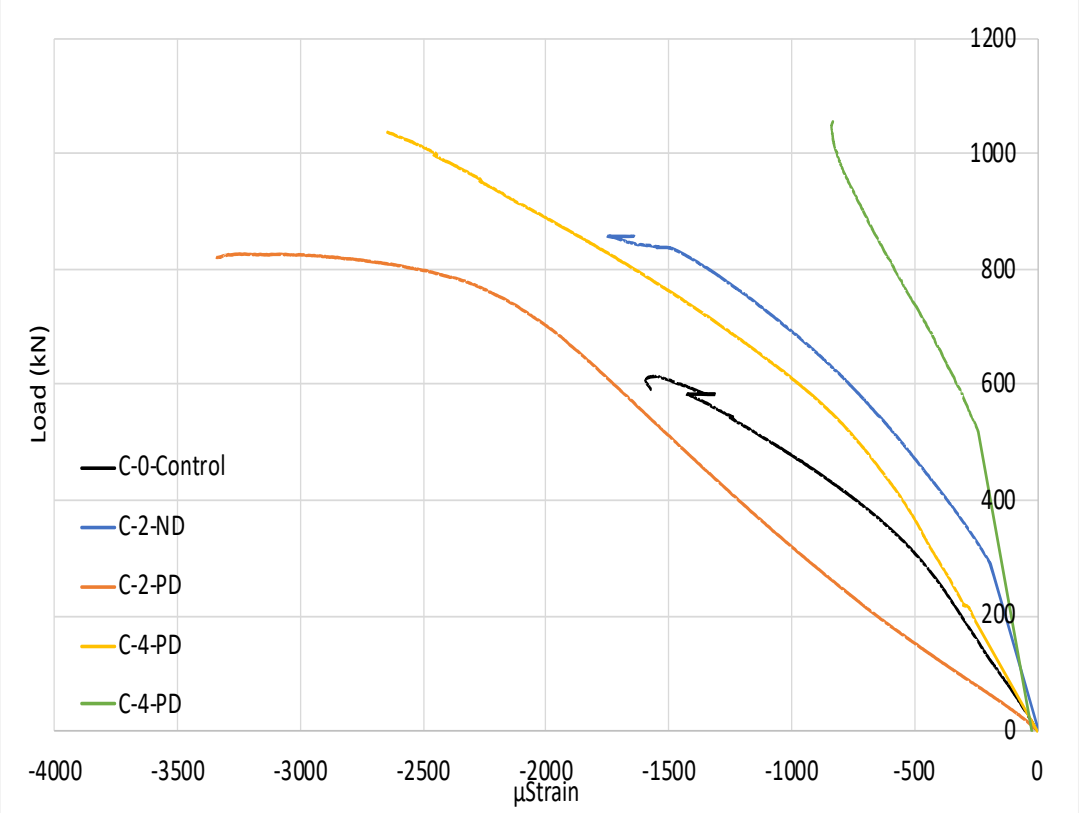

(b)

Figure 30: Load versus vertical concrete strain for (a) Group A and (b) Group B.

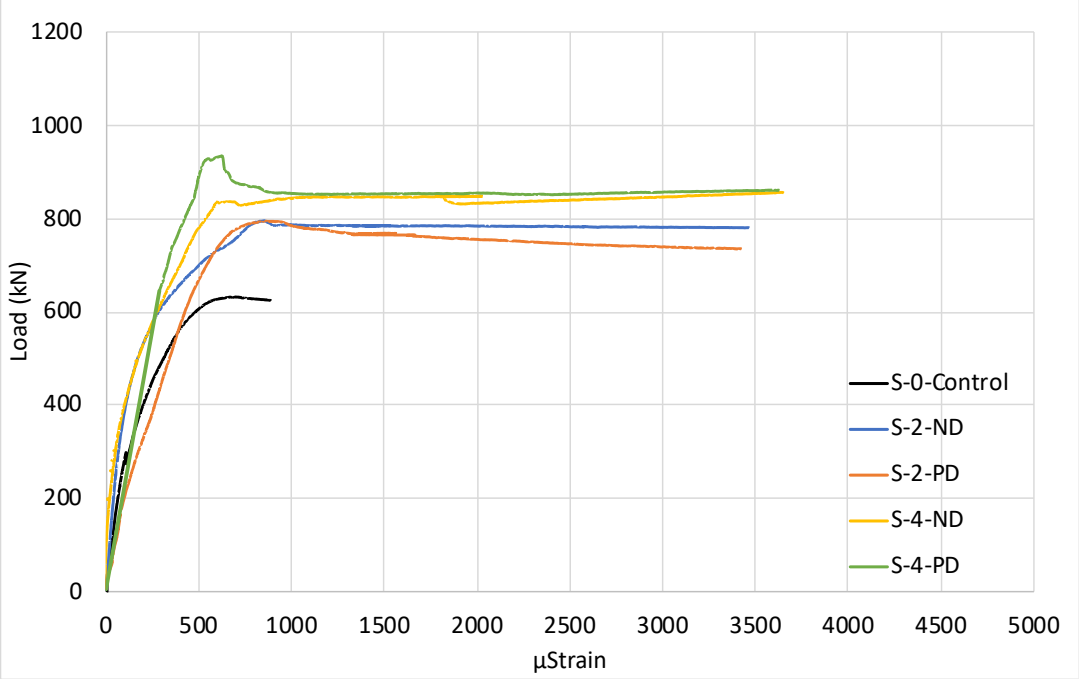

(a)

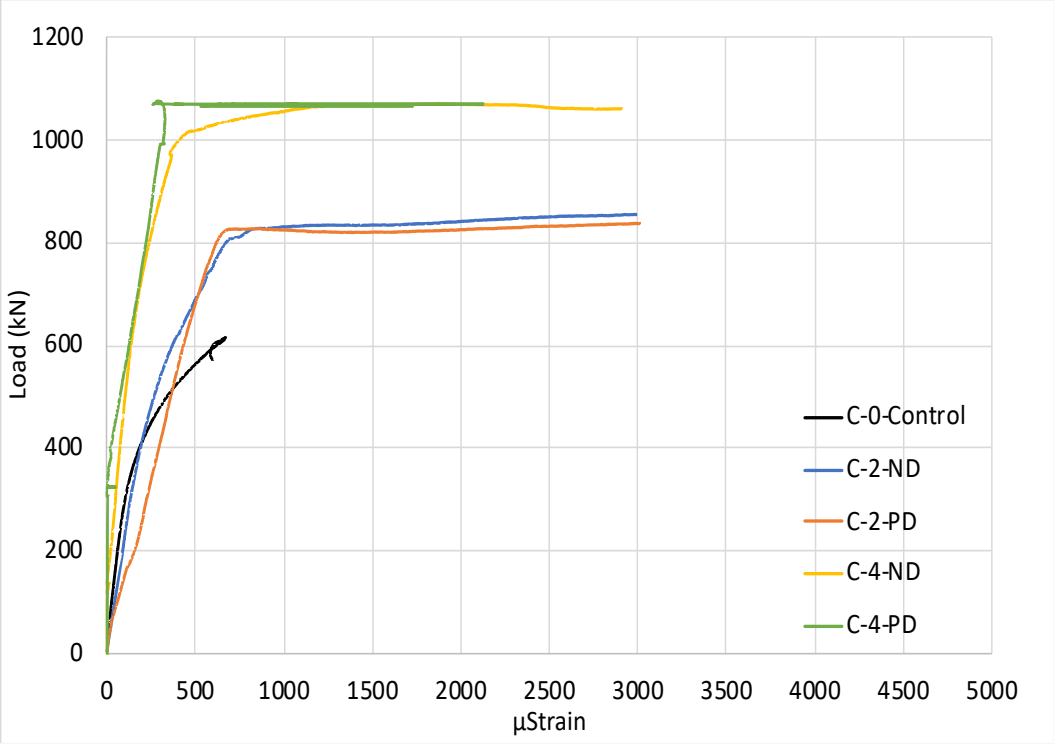

(b)

Figure 31: Load versus horizontal concrete strain for (a) Group A and (b) Group B.

5.4. Failure Modes

In this section, the failure modes for Groups A and B are described in terms of crack propagation, major crack development, concrete spalling, cementitious matrix delamination and PBO mesh rupture.

5.4.1. Group A. The failure modes of Group A columns are shown in Figure 32. For unwrapped column S-0-Control, cracking initiated at the bottom of the columns and propagated upwards. A major diagonal crack occurred at the lower-half region as well as concrete spalling.

Columns wrapped with PBO-FRCM in this group generally exhibited less severe damage at failure, where the damage was more severe for the columns wrapped with 4 PBO-FRCM layers than the ones wrapped with 2 PBO-FRCM layers. The reason behind that is attributed to the higher ability of columns wrapped with 4 layers than 2 layers to resist lateral load, where the confinement level is higher. The failure mode of columns wrapped with 2 PBO-FRCM layers in this group varied. For column S-2-ND,

cracks in the cementitious mortar initiated and propagated at the lower half region of the column. Also, delamination of the outer cementitious matrix layer occurred in multiple locations where the PBO mesh got exposed which revealed the rupture of the mesh. Cracks in column S-2-PD propagated at the middle region where delamination of the outer cementitious mortar occurred around the lower region of the column, and a major vertical crack occurred that exposed the outer ruptured mesh layer.

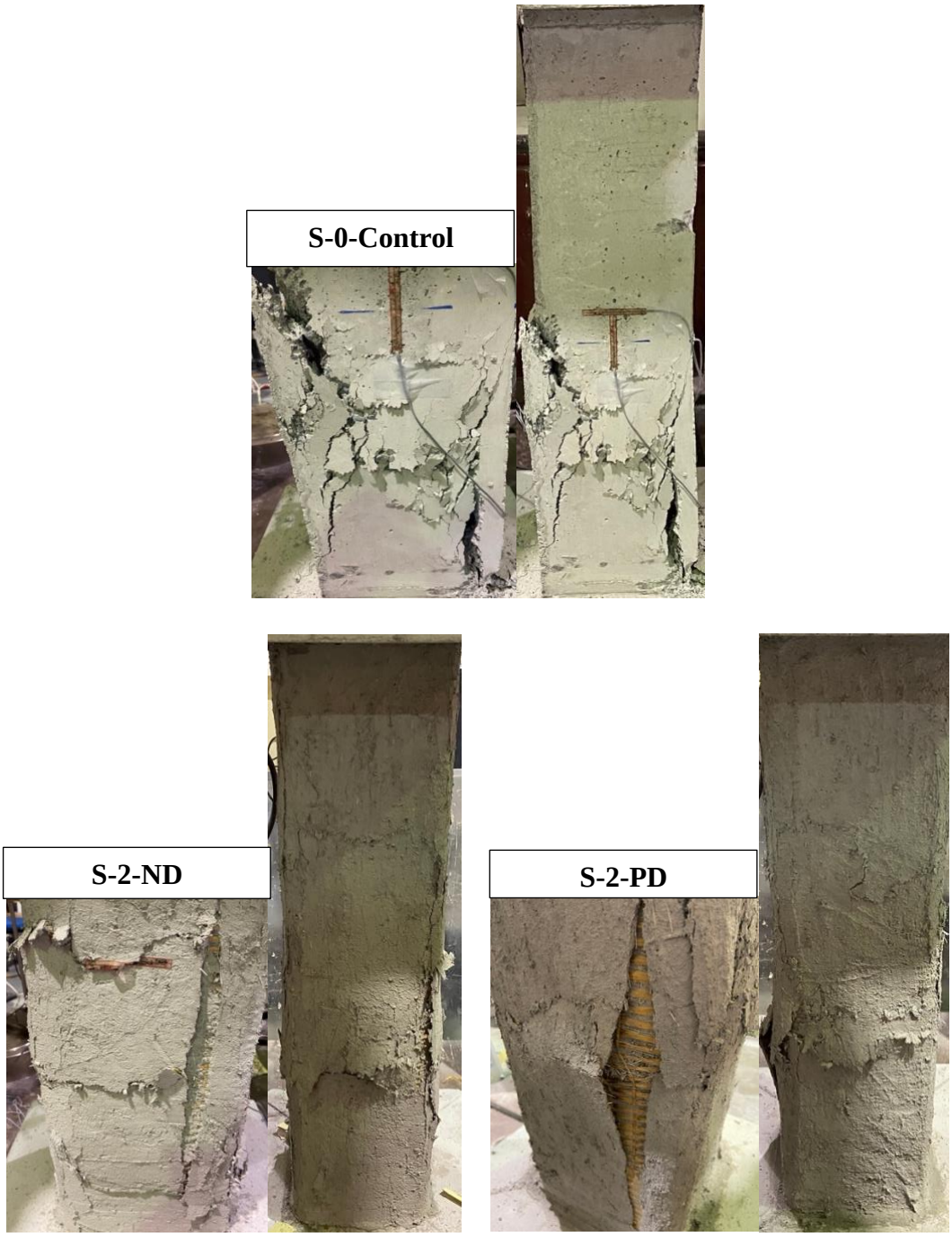

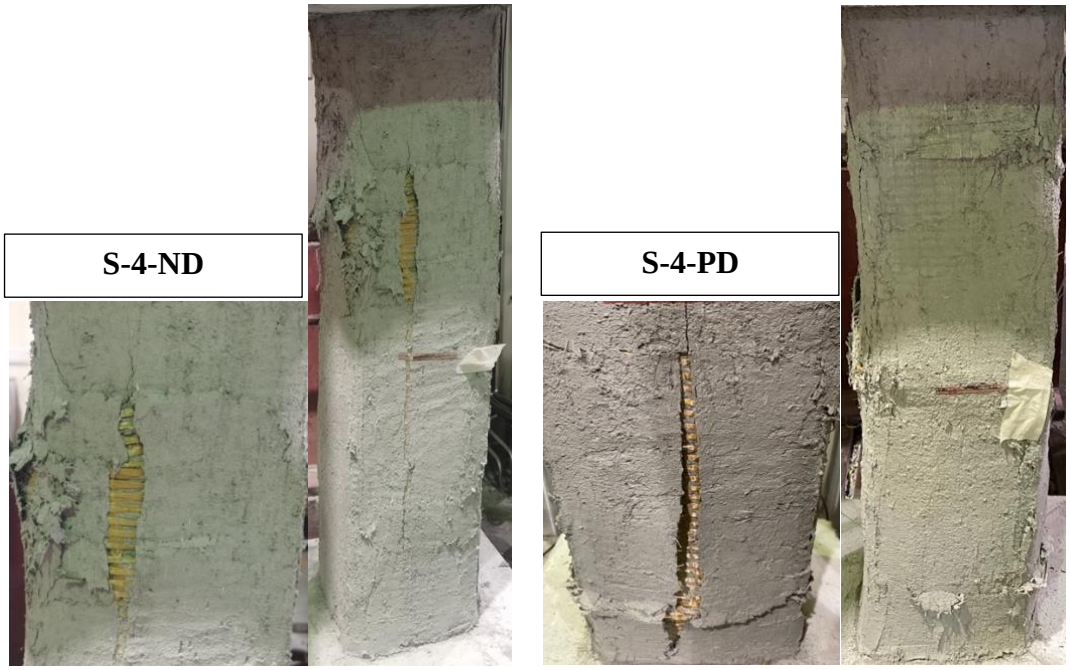

Figure 32: Group A failure modes.

Columns wrapped with 4 PBO-FRCM layers in this group demonstrated a slightly more severe failure than the ones wrapped with 2 PBO-FRCM layers. For column S-4-ND, cracking in cementitious mortar initiated at the upper half region of the column, where a major vertical crack occurred at the middle exposing the ruptured outer mesh layer. For column S-4-PD, a vertical crack occurred along the whole column height slightly exposing the ruptured outer mesh layer. Also, bursting of concrete at the middle region was noticed.

5.4.2. Group B. The failure modes of Group B columns are shown in Figure 33. Cracking in control specimen C-0-Control initiated at the top of the column propagating downwards, and complete concrete clear cover detachment occurred at the upper region of the column.

Similar to Group A, wrapped columns in this group had a less severe failure than the unwrapped ones. However, in this group, columns wrapped with 2 PBO-FRCM layers failed slightly more severely than the ones wrapped with 4 PBO-FRCM layers, as opposed to the previous group. For column C-2-ND, cracks in cementitious mortar occurred and propagated at the upper half of the column and the outer mesh layer was not exposed at any location. Cracks in column C-2-PD propagated and a main vertical

crack in the cementitious matrix occurred at the upper half region where the ruptured outer mesh layer was exposed. Also, delamination of the outer cementitious mortar occurred at some locations.

Columns C-4-ND and C-4-PD failed in a similar manner where cracks initiated and propagated across the columns, and delamination of the outer cementitious matrix layer occurred at the top of the columns that widely exposed the ruptured outer mesh layer.

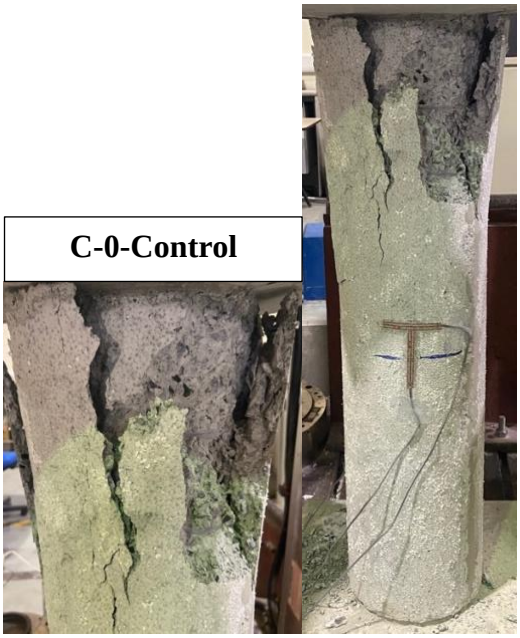

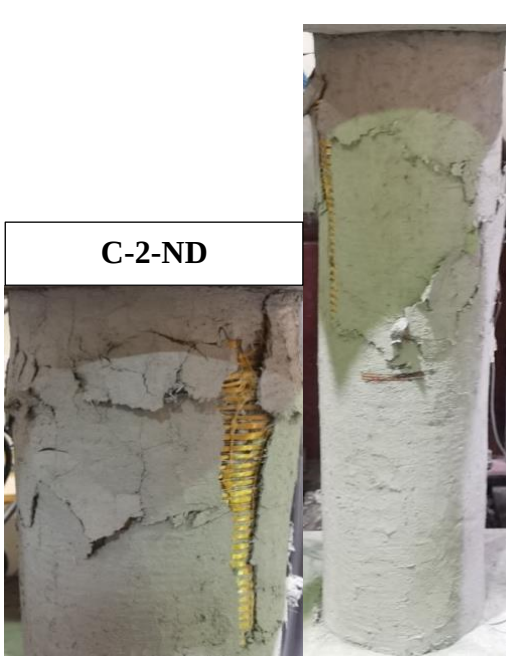

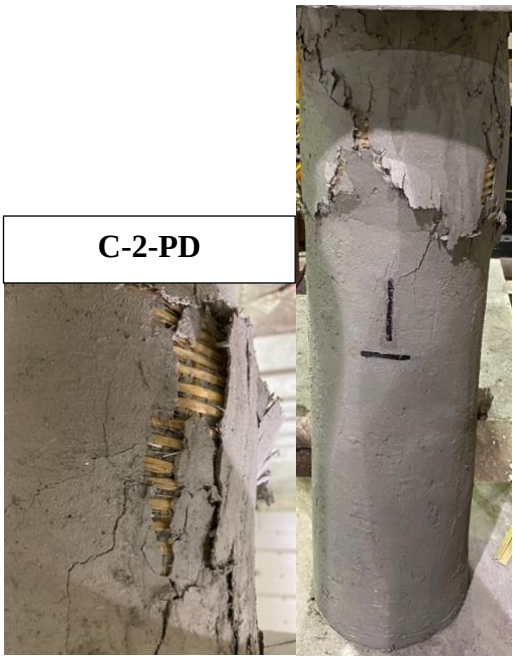

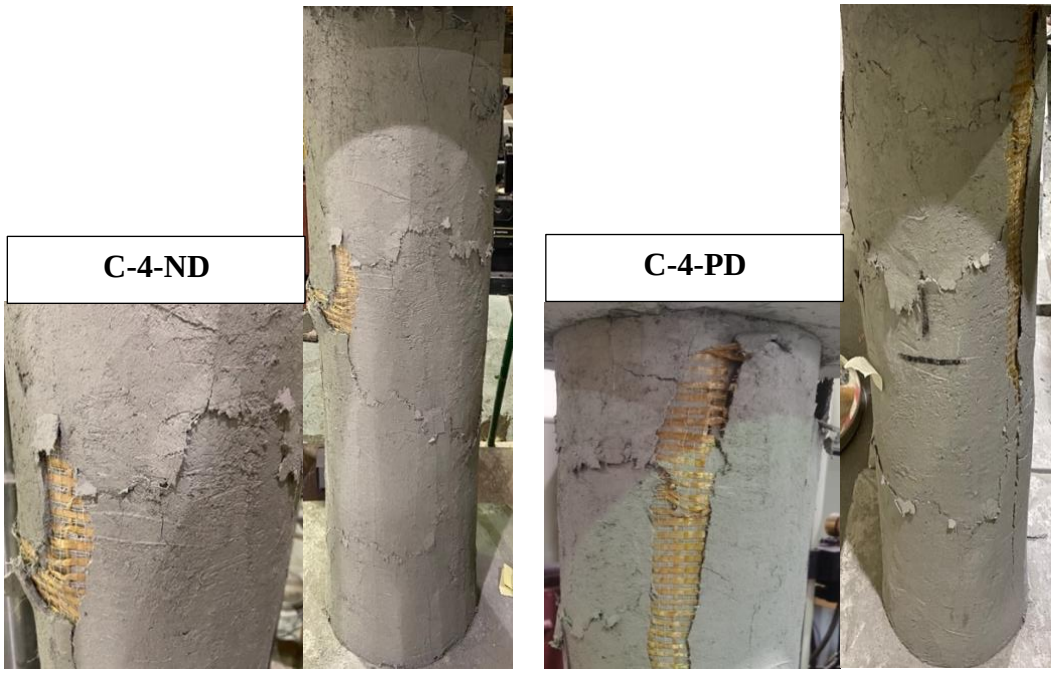

Figure 33: Group B failure modes.

Chapter 6. Discussion of Results

In this chapter, the effects of test parameters (cross-section, number of PBO-FRCM layers and presence of pre-damaging) on the overall behavior of PBO-FRCM strengthened RC columns are discussed in detail. Also, a comparison between the experimental and analytical model results is presented. After that, the performance change of the main study specimens compared to the pilot study is discussed. Lastly, a comparison between this study's results and results from previous work in the literature is presented.

6.1. Effects of Test Parameters on the Overall Behavior of PBO-FRCM Strengthened RC Columns

In this section, the effects of cross-section, number of PBO-FRCM layers and pre-damaging on the behavior of short RC columns strengthened with PBO-FRCM are discussed in terms of increase in ultimate capacity, ductility, failure modes and straining actions.

6.1.1. Effect of cross-section. As clearly shown in Figure 34, circular columns showed a higher increase in capacity than square columns, complying with the known fact that confining circular cross-sections is more effective than confining square ones. The reason behind that is the smooth round perimeter of circular cross-sections, as opposed to square ones where the corners, even after rounding, can cause stress concentrations. All circular columns wrapped with 2 PBO-FRCM layers showed double the capacity increase of square columns wrapped with 2 PBO-FRCM layers, where the capacity increase percentage increased from 20 to 40%. Furthermore, all circular columns wrapped with 4 PBO-FRCM layers showed double the capacity increase of square columns wrapped with 4 PBO-FRCM layers, where the capacity increased from around 35 to 70%.

All wrapped circular columns showed a higher ductility increase than square columns. In clarification, circular columns wrapped with 2 PBO-FRCM layers showed a ductility increase of around 19%, while square columns showed a ductility increase of 31-35%. Also, circular columns wrapped with 4 PBO-FRCM layers showed a ductility increase of around 45-51%, while square columns showed a ductility increase of 80-82%. The failure mode was not affected by the type of cross-section. Similarly,

cross-section type had no effect on strain levels in longitudinal reinforcement, longitudinal concrete and transverse concrete. However, cross-section type had an effect on middle tie strain, as strain levels reached by the middle ties of square columns were considerably higher than those reached by the middle ties of circular columns, where the stiffness of the load versus μStrain curve for most circular columns was very large.

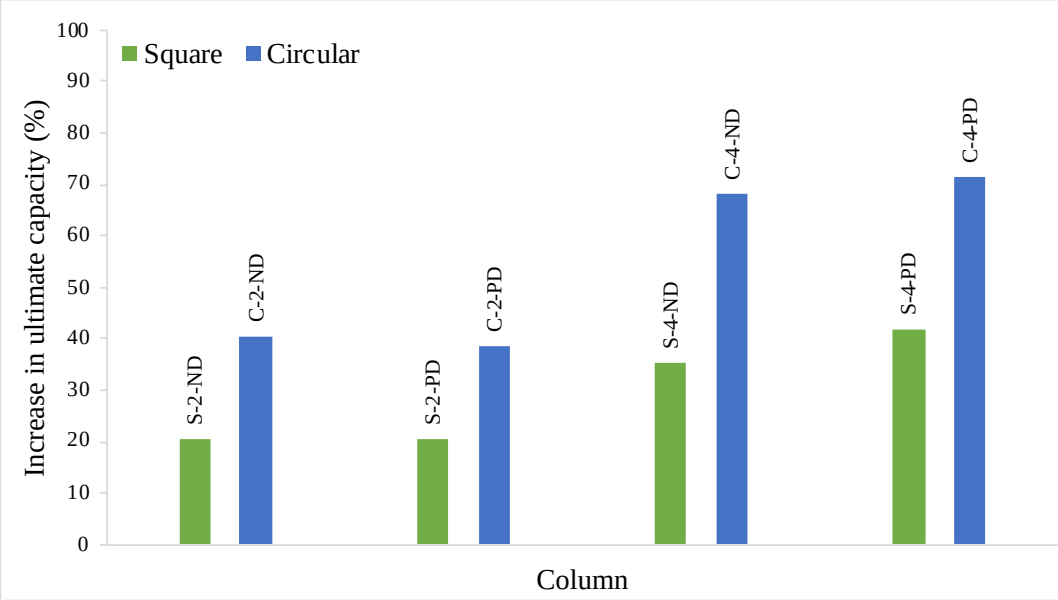

Figure 34: Ultimate capacity comparison between columns with different cross-sections.

6.1.2. Effect of number of PBO-FRCM layers. All columns wrapped with 4 PBO-FRCM layers showed an increased capacity considerably higher than the ones wrapped with 2 PBO-FRCM layers, as clearly shown in Figure 35. For square columns, the difference in capacity increase and ultimate load between columns wrapped with 2 and 4 PBO-FRCM layers was around 14-21% and 95-140 kN, respectively. For circular columns, the difference in capacity increase between columns wrapped with 2 and 4 PBO-FRCM layers was around 28-33% and 173-202 kN, respectively.

All columns strengthened with 4 PBO-FRCM layers showed considerably higher ductility than the ones strengthened with 2 PBO-FRCM layers, where the difference in ductility increase between square columns strengthened with 2 and 4 PBO-FRCM layers was 26-32%, while it was 45-51% for circular columns. This shows

that increasing the number of PBO-FRCM layers increases the ductility significantly, where the increase is more pronounce in circular columns than square ones. The failure mode for all columns wrapped with 2 PBO-FRCM layers was more severe than the ones wrapped with 4 PBO-FRCM layers, where the cracks in cementitious mortar were wider and the outer mesh layer was more exposed and damaged. The number of PBO-FRCM layers had no effect on strain levels in longitudinal reinforcement, longitudinal concrete, transverse concrete and middle ties.

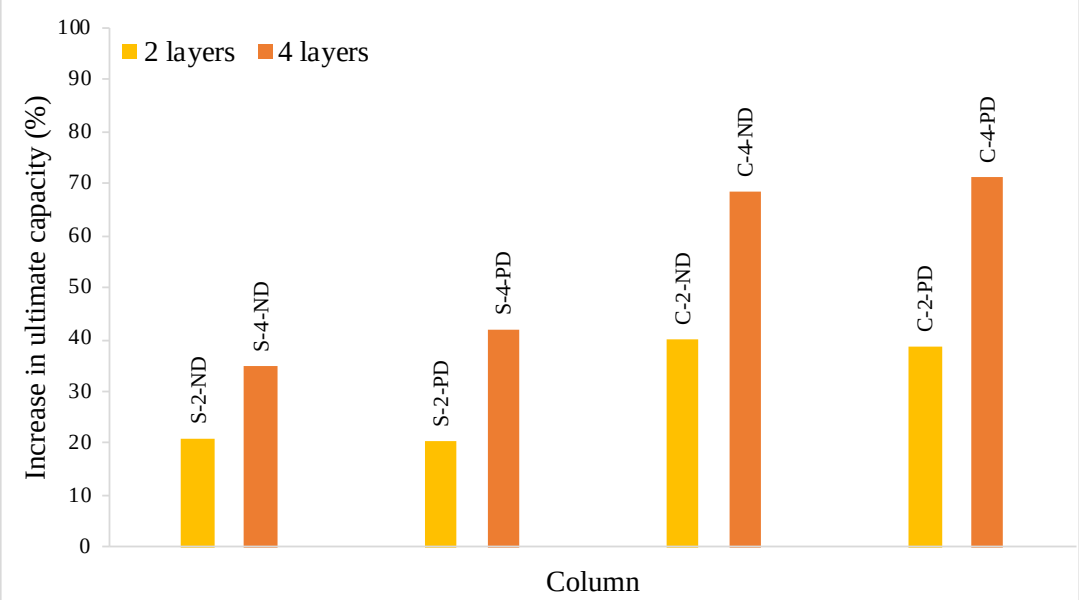

Figure 35: Ultimate capacity comparison between columns wrapped with a different number of PBO-FRCM layers.

6.1.3. Effect of pre-damaging. Wrapping pre-damaged columns with PBO-FRCM successfully restored 100% of their original capacity and enhanced it even further. As shown in Figure 36, most wrapped pre-damaged columns reached an increase in ultimate capacity equal to or slightly different from that reached by their non-damaged counterparts, indicating the high efficiency of wrapping pre-damaged RC columns with PBO-FRCM.

Pre-damaging had no clear effect on the ductility of strengthened columns. Also, pre-damaging had no clear effect on the failure modes of the columns wrapped after pre-damaging when compared to the failure modes of non-damaged wrapped

columns. Pre-damaging had no effect on strain levels in longitudinal reinforcement, longitudinal concrete, transverse concrete and middle ties.

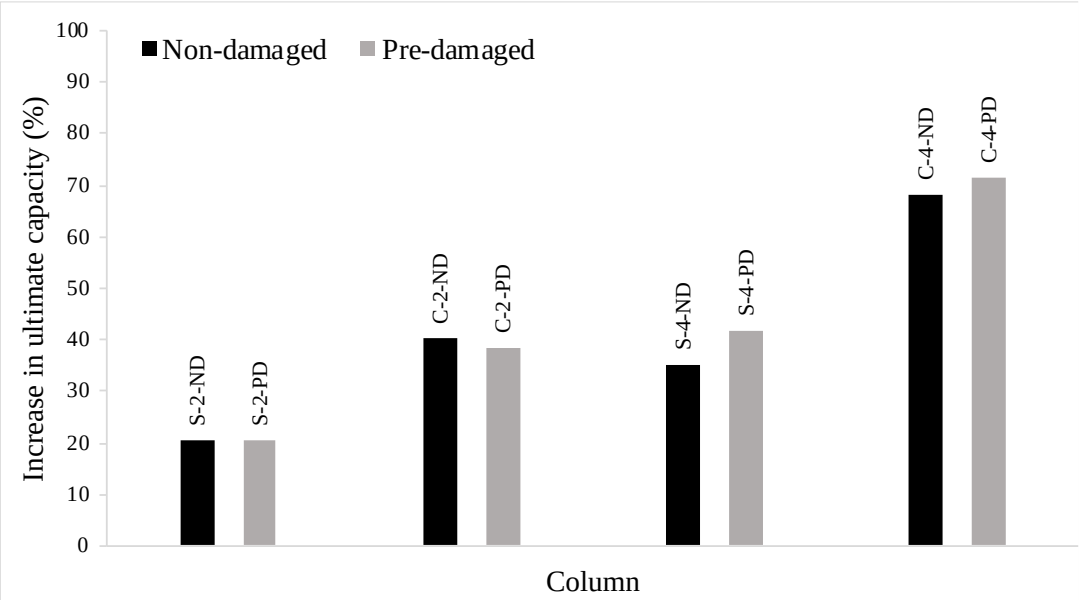

Figure 36: Ultimate capacity comparison between non-damaged and pre-damaged columns.

6.2. Analytical Prediction of Ultimate Capacity

ACI 318-19 provisions [48] were used to obtain the nominal capacity of the control unstrengthened columns of the experimental program, while ACI 549.4R-13 provisions [15] were used to obtain the nominal capacity of the control strengthened columns. For unstrengthened columns, Equation 3 from Chapter 3 was used to calculate the capacity for both square and circular columns. However, the capacity calculation for strengthened columns differed based on the type of cross-section according to ACI 549.4R-13 provisions [15]. For square columns, Equations 5 and 6 were used to calculate the efficiency factor (κ_a). For circular columns, the value of κ_a was directly taken as 1.0. Equations 7 and 8 were used to find the confining pressure due to FRCM (f_l) for square and circular columns, respectively. Equation 9 shows a limitation set for the ultimate axial compressive strain of confined concrete (ε_{ccu}), where it should not exceed 0.01. Based on the aforementioned limitation, f_l calculated from Equations 7 and 8 and used to find the maximum confined concrete compressive strength (f'_{cc}) from Equation 10 should not exceed that obtained from Equation 9 corresponding to

ε_{ccu} equal to 0.01. Equation 11 was used to calculate the nominal compressive strength ($P_{n)}$ for strengthened columns.

$$\frac{A_e}{A_c} = \frac{1 - \frac{\left[\left(\frac{b}{h}\right)(h-2r_c)^2 + \left(\frac{h}{b}\right)(b-2r_c)^2\right]}{3A_g} - \rho_g}{1-\rho_g} \quad (5)$$

$$\kappa_a = \frac{A_e}{A_c}\left(\frac{b}{h}\right)^2 \quad (6)$$

$$f_l = \frac{2nA_f E_f \varepsilon_{fe}}{\sqrt{b^2+h^2}}, \varepsilon_{fe} = smaller\ of(\varepsilon_{fe}, 0.012) \quad (7)$$

$$f_l = \frac{2nA_f E_f \varepsilon_{fe}}{D}, \varepsilon_{fe} = smaller\ of\left(\varepsilon_{fe}, 0.012\right) \quad (8)$$

$$\varepsilon_{ccu} = \varepsilon'_c\left(1.5 + 12\kappa_b \frac{f_l}{f'_c}\left(\frac{\varepsilon_{fe}}{\varepsilon'_c}\right)^{0.45}\right) \leq 0.01 \quad (9)$$

$$f'_{cc} = f'_c + 3.1\kappa_a f_l \quad (10)$$

$$P_n = A_s f_y + 0.85 f'_{cc}\left(A_g - A_s\right) \quad (11)$$

where A_e is the area of effectively confined concrete, A_c is the net cross-sectional area of compression member, b is the short side dimension of compression member with rectangular cross-section, h is the long side dimension of compression member with rectangular cross-section, r_c is the radius of edges of a rectangular cross section confined with FRCM, A_g is the gross cross-sectional area of compression member, ρ_g is the ratio of the area of longitudinal steel reinforcement to the cross-sectional area of a compression member, κ_a is the efficiency factor for FRCM reinforcement in the determination of f'_{cc}, f_l is the maximum confining pressure due to FRCM jacket, n is the number of layers of mesh reinforcement, A_f is the area of mesh reinforcement by unit width, E_f is the tensile modulus of elasticity of cracked FRCM, ε_{fe} is the effective tensile strain level in FRCM composite material attained at failure, D is the diameter of compression member, f'_{cc} is the maximum compressive strength of confined concrete, f'_c is the specified compressive strength of concrete, P_n is the nominal axial strength, A_s is the area of longitudinal steel reinforcement and f_y is the steel tensile yield strength.

Table 12 shows a comparison between the experimental ($Pu_{experimental}$) and analytical (Pn) results of the ultimate capacity of all control specimens. The nominal ultimate capacities of unstrengthened control columns were lower than the experimental ones by around 14-19%. The difference between predicted and

experimental capacities may be attributed to a variation between actual properties of materials of the tested large-scale columns, and those used in the analysis, which were based on data of concrete samples and steel coupons. For strengthened columns, the nominal ultimate capacities were very close to the experimental ones, where the nominal ultimate capacities of all strengthened columns were equal to or lower than the experimental ones by around 4-7%, except for columns S-2-ND, where the nominal capacity was higher than the experimental one by 2% only. This shows that the ACI 549.4R-13 code is generally accurate for estimating the capacity of columns strengthened with FRCM.

Table 12: Experimental versus analytical results.

Specimen	**$Pu_{experimental}$ (kN)**	**Pn (kN)**	**$Pu_{experimental}$/Pn**
S-0-Control	660.1	765.6	0.86
S-2-ND	796.7	812.0	0.98
S-4-ND	891.7	858.3	1.04
C-0-Control	615.2	757.5	0.81
C-2-ND	862.5	865.2	1.00
C-4-ND	1035.8	970.1	1.07

6.3. Performance-Based Changes and Modifications from the Pilot Study

The specimen fabrication of the main study was developed based on results and outcomes of the pilot study. The main modified parameters were the cross-section dimensions, concrete clear cover, tie spacing, and the technique used to prevent premature failure, as summarized in Table 6 in Chapter 3. By keeping the same size and number of rebars, the longitudinal steel reinforcement ratio was slightly reduced due the increase in cross-sectional area. Also, a new important parameter investigating the performance of FRCM strengthened pre-damaged columns was introduced in the main study.

The main reason behind increasing the cross-sectional dimensions and concrete clear cover was to facilitate the concrete casting process, as some problems were faced during casting the pilot study specimens due to the small dimensions and clear cover.

The aforementioned modifications were successful in easing the concrete casting process, where the process went smoothly, and no problems occurred.

The 75 mm tie spacing used in the pilot study was chosen to be half of the square cross-section side dimension, which was 150 mm. The tie spacing for the main study was increased to 90 mm in order to follow the same technique as the pilot study, where the square cross-section side dimension for the main study was 180 mm. Consequently, no change of behavior was observed from increasing the tie spacing.

In the pilot study, the tie spacing was reduced at the column ends in order to prevent the occurrence of stress concentrations at the end that might cause premature failure of the columns. However, one specimen in the pilot study failed by premature failure due to stress concentrations at the column ends, which led to the modification of the technique used to prevent such failure. For the main study, the use of end corbels was introduced as mentioned in Chapter 4 and shown in Figure 10. The use of end corbels was successful in preventing premature failure of all column specimens.

6.4. Comparison of Experimental Results with Previous Work

As previously mentioned in the literature review in Chapter 2, Toska et al. [44] investigated the behavior of pre-damaged short RC columns strengthened with C-FRCM under monotonic loading. The main study of this thesis was compared to the experimental study by Toska et al. [44] in terms of degree of pre-damage, capacity restoration for pre-damaged columns, and the effect of cross-section type on the ultimate capacity and transverse steel reinforcement (TSR) strain. Since the study by Toska et al. [44] only included columns wrapped with 2 FRCM layers, only the columns wrapped with 2 layers from the main study were included in this comparison.

Table 13 shows a summarized comparison between the study by Toska et al. [44] and the main study of this thesis. Similar to the main study of this thesis, the capacity of all pre-damaged columns from the study by Toska et al. [44], except for one, was restored after strengthening with FRCM and further improved by a range of 1-34%, as opposed to the main study of this thesis where the improvement range was 21-39%. Only one square columns from the study by Toska et al. [44] did not regain a 100% of the original capacity, where only 90% of the capacity was restored. The reason behind that could be attributed to the low tie spacing of that column, where the tie

spacing was varied across the specimens in Toska's study. Moreover, the effect of cross-section type on the ultimate capacity and TSR strain was similar to Toska's study. Circular columns showed a higher improvement in ultimate capacity for both non-damaged and pre-damaged specimens, with a range of 20 to 30% improvement difference between circular and square columns. Additionally, both studies showed a similar TSR strain behavior, where both non-damaged and pre-damaged square columns exhibited higher TSR strains than circular ones.

Table 13: Summary of comparison between main study and previous work.

	$f'c$ (MPa)	H (mm)	AxB (mm x mm)	D (mm)	ρ_s (%)	Ties		Type of FRCM system	Degree of pre-damage (%)	Strength increase due to FRCM (%)	Difference in capacity improvement between circular and square columns (%)	Columns with higher TSR strains
						Bar size (mm)	S (mm)					
Toska et al. [44]	21	1000	300x300	300	0.68	8	200, 300	C-FRCM	70	-10 to 34	30%	Square
Main study	20	800	180x180	200	1.5	6	90	PBO-FRCM	100	20 to 40	20%	Square

$f'c$= concrete compressive strength; H= column height; AxB= square cross-section dimensions; D= circular cross-section diameter; ρ_s= longitudinal steel reinforcement ratio; S= tie spacing.

Chapter 7. Conclusion and Future Work

In this thesis, the overall behavior of pre-damaged short RC columns strengthened with PBO-FRCM under concentric loading was investigated. A total of 10 columns were cast and divided into 2 main groups, where the investigated parameters included the type of cross-section (square versus circular), number of PBO-FRCM layers (0, 2 and 4 layers) and the presence of pre-damaging. All columns were subjected to monotonic concentric loading till failure using a UTM. The effects of test parameters on the behavior of short RC columns were investigated in terms of ultimate capacity, ductility, failure modes and straining actions. The main conclusions drawn from the experimental results are as follows:

- Strengthening of short RC columns with PBO-FRCM improved the ultimate capacity and ductility of both non-damaged and pre-damaged columns.
- Circular columns showed a higher increase in capacity than square columns, where the difference ranged from 18-33%, confirming that confining circular cross-sections is more effective than square ones.
- Ductility increase due to PBO-FRCM wrapping was higher for circular columns than square columns, where the difference ranged between 12-31%.
- Columns wrapped with 4 PBO-FRCM layers showed a higher increase in ultimate capacity than the ones wrapped with 2 layers. The difference in capacity increase ranged from 14 to 21% for square columns and 28 to 33% for circular columns.
- Ductility increased with the increase of number of PBO-FRCM layers, where the increase was more pronounced in circular columns.
- The ultimate capacity of all pre-damaged columns was restored and further improved compared to the control columns.
- Ductility was not affected by the presence of pre-damaging.
- The failure modes were not affected by the type of cross-section or presence of pre-damaging, while they were affected by the number of PBO-FRCM layers, where the failure mode of all columns wrapped with 2 PBO-FRCM layers was more severe than that of the ones wrapped with 4 PBO-FRCM layers.

- The comparison between experimental results and theoretical predictions of ultimate capacity showed that ACI 549.4R-13 [15] code is accurate for predicting the axial capacity of short RC columns strengthened with PBO-FRCM.

The experimental results of this study showed a promising future for the use of FRCM systems in rehabilitating existing deteriorated RC columns, where the following recommendations are suggested for future studies:

- This study was successful in investigating the behavior of short RC columns strengthened with PBO-FRCM after sustaining pre-damaging procedures where columns were monotonically subjected to 100% of the ultimate load. It is recommended to conduct future studies that investigate the seismic performance of short RC columns strengthened with FRCM.
- It is recommended to study the effect of varying the tie spacing on the behavior of RC columns strengthened with FRCM.
- It is recommended to use the experimental results presented in this study to verify and develop a finite element model in order to expand the parametric analysis conducted in this study.

References

[1] "Reinforced concrete jacketing," *Weber Middle East*, 2021. https://www.middleeast.weber/concrete-repair-anchoring-and-grouting/reinforced-concrete-jacketing (accessed Mar. 14, 2021).

[2] A. Ahmad, M. Elchalakani, N. Elmesalami, A. El Refai, and F. Abed, "Reliability analysis of strength models for short-concrete columns under concentric loading with FRP rebars through Artificial Neural Network," *J. Build. Eng.*, vol. 42, no. March, p. 102497, 2021, doi: 10.1016/j.jobe.2021.102497.

[3] F. Abed, Z. Mehaini, C. Oucif, A. Abdul–Latif, and R. Baleh, "Quasi-static and dynamic response of GFRP and BFRP bars under compression," *Compos. Part C Open Access*, vol. 2, no. June, p. 100034, 2020, doi: 10.1016/j.jcomc.2020.100034.

[4] M. Al Rifai, H. El-Hassan, T. El-Maaddawy, and F. Abed, "Durability of basalt FRP reinforcing bars in alkaline solution and moist concrete environments," *Constr. Build. Mater.*, vol. 243, p. 118258, 2020, doi: 10.1016/j.conbuildmat.2020.118258.

[5] H. Wang and A. Belarbi, "Ductility characteristics of fiber-reinforced-concrete beams reinforced with FRP rebars," *Constr. Build. Mater.*, vol. 25, no. 5, pp. 2391–2401, 2011, doi: 10.1016/j.conbuildmat.2010.11.040.

[6] N. Elmesalami, F. Abed, and A. El Refai, "Concrete Columns Reinforced with GFRP and BFRP Bars under Concentric and Eccentric Loads: Experimental Testing and Analytical Investigation," *J. Compos. Constr.*, vol. 25, no. 2, p. 04021003, 2021, doi: 10.1061/(asce)cc.1943-5614.0001115.

[7] F. Abed, M. Al-Mimar, and S. Ahmed, "Performance of BFRP RC beams using high strength concrete," *Compos. Part C Open Access*, vol. 4, no. January, p. 100107, 2021, doi: 10.1016/j.jcomc.2021.100107.

[8] B. Abdul-Salam, A. S. Farghaly, and B. Benmokrane, "Mechanisms of shear resistance of one-way concrete slabs reinforced with FRP bars," *Constr. Build. Mater.*, vol. 127, pp. 959–970, 2016, doi: 10.1016/j.conbuildmat.2016.10.015.

[9] N. Elmessalami, A. El Refai, and F. Abed, "Fiber-reinforced polymers bars for compression reinforcement: A promising alternative to steel bars," *Constr. Build. Mater.*, vol. 209, pp. 725–737, 2019, doi: 10.1016/j.conbuildmat.2019.03.105.

[10] F. Abed, C. Oucif, Y. Awera, H. H. Mhanna, and H. Alkhraisha, "FE modeling of concrete beams and columns reinforced with FRP composites," *Def. Technol.*, vol. 17, no. 1, pp. 1–14, 2021, doi: 10.1016/j.dt.2020.02.015.

[11] P. Escórcio and P. M. França, "Experimental study of a rehabilitation solution that uses GFRP bars to replace the steel bars of reinforced concrete beams," *Eng. Struct.*, vol. 128, pp. 166–183, 2016, doi: 10.1016/j.engstruct.2016.09.013.

[12] K. S. Elango, R. Gopi, C. Jayaguru, D. Vivek, R. Saravanakumar, and V.

Rajeshkumar, “Experimental investigation on concrete beams reinforced with basalt fiber reinforced polymer bars,” *Materials Today: Proceedings*, vol. 45, pp. 2426-2429, 2020, doi: 10.1016/j.matpr.2020.10.840.

[13] L. Alnajmi and F. Abed, “Evaluation of FRP bars under compression and their performance in RC columns,” *Materials (Basel).*, vol. 13, no. 20, pp. 1–19, 2020, doi: 10.3390/ma13204541.

[14] F. Abed and A. R. Alhafiz, “Effect of basalt fibers on the flexural behavior of concrete beams reinforced with BFRP bars,” *Compos. Struct.*, vol. 215, no. January, pp. 23–34, 2019, doi: 10.1016/j.compstruct.2019.02.050.

[15] American Concrete Institute (ACI), *Guide to Design and Construction of Externally Bonded Fabric-Reinforced Cementitious Matrix (FRCM) Systems for Repair and Strengthening Concrete and Masonry Structures*, ACI 549.4R. Farmington Hills, MI, USA: American Concrete Institute, 2013.

[16] A. D’Ambrisi, L. Feo, and F. Focacci, “Experimental analysis on bond between PBO-FRCM strengthening materials and concrete,” *Compos. Part B Eng.*, vol. 44, no. 1, pp. 524–532, 2013, doi: 10.1016/j.compositesb.2012.03.011.

[17] A. Younis and U. Ebead, “Bond characteristics of different FRCM systems,” *Constr. Build. Mater.*, vol. 175, pp. 610–620, 2018, doi: 10.1016/j.conbuildmat.2018.04.216.

[18] T. Trapko, “Behaviour of fibre reinforced cementitious matrix strengthened concrete columns under eccentric compression loading,” *Mater. Des.*, vol. 54, pp. 947–954, 2014, doi: 10.1016/j.matdes.2013.09.008.

[19] M. J. Kim, H. G. Kim, Y. J. Lee, D. H. Kim, M. S. Jo, and K. H. Kim, “Evaluation of bond properties of a fabric-reinforced cementitious matrix for strengthening of concrete structures,” *Appl. Sci.*, vol. 10, no. 11, 2020, doi: 10.3390/app10113767.

[20] M. Zhu, J. H. Zhu, T. Ueda, K. Matsumoto, and M. Su, “Bond behavior of carbon fabric reinforced cementitious matrix (FRCM) composites considering matrix impregnation,” *Compos. Struct.*, vol. 262, no. June 2020, p. 113350, 2021, doi: 10.1016/j.compstruct.2020.113350.

[21] A. S. Calabrese, T. D’Antino, P. Colombi, and C. Poggi, “Study of the influence of interface normal stresses on the bond behavior of FRCM composites using direct shear and modified beam tests,” *Constr. Build. Mater.*, vol. 262, p. 120029, 2020, doi: 10.1016/j.conbuildmat.2020.120029.

[22] X. Wang, C. C. Lam, B. C. Sun, T. Noguchi, and V. P. Iu, “Effect of curing environment on the tensile behaviour of FRCM composites,” *Constr. Build. Mater.*, vol. 238, p. 117729, 2020, doi: 10.1016/j.conbuildmat.2019.117729.

[23] J. Donnini, F. Bompadre, and V. Corinaldesi, “Tensile behavior of a glass FRCM system after different environmental exposures,” *Processes*, vol. 8, no. 9, 2020, doi: 10.3390/pr8091074.

[24] M. Su, L. Wei, J.-H. Zhu, T. Ueda, G. Guo, and F. Xing, “Combined Impressed Current Cathodic Protection and FRCM Strengthening for Corrosion-Prone

Concrete Structures," *J. Compos. Constr.*, vol. 23, no. 4, p. 04019021, 2019, doi: 10.1061/(asce)cc.1943-5614.0000949.

[25] E. Franzoni, C. Gentilini, M. Santandrea, S. Zanotto, and C. Carloni, "Durability of steel FRCM-masonry joints: effect of water and salt crystallization," *Mater. Struct. Constr.*, vol. 50, no. 4, pp. 1–16, 2017, doi: 10.1617/s11527-017-1070-2.

[26] A. M. Turk, "Seismic response analysis of masonry minaret and possible strengthening by fiber reinforced cementitious matrix (FRCM) materials," *Adv. Mater. Sci. Eng.*, vol. 2013, 2013, doi: 10.1155/2013/952497.

[27] F. G. Carozzi, G. Milani, and C. Poggi, "Mechanical properties and numerical modeling of Fabric Reinforced Cementitious Matrix (FRCM) systems for strengthening of masonry structures," *Compos. Struct.*, vol. 107, pp. 711–725, 2014, doi: 10.1016/j.compstruct.2013.08.026.

[28] F. S. Murgo and C. Mazzotti, "Masonry columns strengthened with FRCM system: Numerical and experimental evaluation," *Constr. Build. Mater.*, vol. 202, pp. 208–222, 2019, doi: 10.1016/j.conbuildmat.2018.12.211.

[29] A. Jabr, A. El-Ragaby, and F. Ghrib, "Effect of the fiber type and axial stiffness of FRCM on the flexural strengthening of RC beams," *Fibers*, vol. 5, no. 1, pp. 2, 2017, doi: 10.3390/fib5010002.

[30] L. H. Sneed, S. Verre, C. Carloni, and L. Ombres, "Flexural behavior of RC beams strengthened with steel-FRCM composite," *Eng. Struct.*, vol. 127, pp. 686–699, 2016, doi: 10.1016/j.engstruct.2016.09.006.

[31] H. Akbari Hadad, A. Nanni, U. A. Ebead, and A. El Refai, "Static and Fatigue Performance of FRCM-Strengthened Concrete Beams," *J. Compos. Constr.*, vol. 22, no. 5, p. 04018033, 2018, doi: 10.1061/(asce)cc.1943-5614.0000868.

[32] M. Elghazy, A. El Refai, U. A. Ebead, and A. Nanni, "Performance of corrosion-aged Reinforced Concrete (RC) beams rehabilitated with Fabric-Reinforced Cementitious Matrix (FRCM) ", in *4th international conference in Sustainable Construction Materials and Technologies (SCMT4)*, Las Vegas, Nevada, USA, 2016.

[33] A. Younis, U. Ebead, and K. C. Shrestha, "Different FRCM systems for shear-strengthening of reinforced concrete beams," *Constr. Build. Mater.*, vol. 153, pp. 514–526, 2017, doi: 10.1016/j.conbuildmat.2017.07.132.

[34] A. Younis, U. Ebead, and K. C. Shrestha, "FRCM shear strengthening for concrete beams," *ISEC 2017 - 9th Int. Struct. Eng. Constr. Conf. Resilient Struct. Sustain. Constr.*, no. August, 2017, doi: 10.14455/isec.res.2017.175.

[35] R. Azam and K. Soudki, "FRCM Strengthening of Shear-Critical RC Beams," *J. Compos. Constr.*, vol. 18, no. 5, p. 04014012, 2014, doi: 10.1061/(asce)cc.1943-5614.0000464.

[36] G. Loreto, S. Babaeidarabad, L. Leardini, and A. Nanni, "RC beams shear-strengthened with fabric-reinforced-cementitious-matrix (FRCM) composite," *Int. J. Adv. Struct. Eng.*, vol. 7, no. 4, pp. 341–352, 2015, doi: 10.1007/s40091-015-0102-9.

[37] Z. R. Aljazaeri and J. J. Myers, “Strengthening of Reinforced-Concrete Beams in Shear with a Fabric-Reinforced Cementitious Matrix,” *J. Compos. Constr.*, vol. 21, no. 5, p. 04017041, 2017, doi: 10.1061/(asce)cc.1943-5614.0000822.

[38] D. Marcinczak, T. Trapko, and M. Musiał, “Shear strengthening of reinforced concrete beams with PBO-FRCM composites with anchorage,” *Compos. Part B Eng.*, vol. 158, no. August 2018, pp. 149–161, 2019, doi: 10.1016/j.compositesb.2018.09.061.

[39] H. Akbari Hadad, B. Erickson, and A. Nanni, “Flexural analysis and design of FRCM-strengthened RC beams,” *Constr. Build. Mater.*, vol. 244, p. 118371, 2020, doi: 10.1016/j.conbuildmat.2020.118371.

[40] P. Colajanni, F. De Domenico, A. Recupero, and N. Spinella, “Concrete columns confined with fibre reinforced cementitious mortars: Experimentation and modelling,” *Constr. Build. Mater.*, vol. 52, pp. 375–384, 2014, doi: 10.1016/j.conbuildmat.2013.11.048.

[41] P. Colajanni, M. Fossetti, and G. MacAluso, “Effects of confinement level, cross-section shape and corner radius on the cyclic behavior of CFRCM confined concrete columns,” *Constr. Build. Mater.*, vol. 55, pp. 379–389, 2014, doi: 10.1016/j.conbuildmat.2014.01.035.

[42] F. Faleschini, M. A. Zanini, L. Hofer, and C. Pellegrino, “Experimental behavior of reinforced concrete columns confined with carbon-FRCM composites,” *Constr. Build. Mater.*, vol. 243, p. 118296, 2020, doi: 10.1016/j.conbuildmat.2020.118296.

[43] R. Feng, Y. Li, J. H. Zhu, and F. Xing, “Behavior of corroded circular RC columns strengthened by C-FRCM under cyclic loading,” *Eng. Struct.*, vol. 226, no. October 2020, p. 111311, 2021, doi: 10.1016/j.engstruct.2020.111311.

[44] K. Toska, F. Faleschini, M. A. Zanini, L. Hofer, and C. Pellegrino, “Repair of severely damaged RC columns through FRCM composites,” *Constr. Build. Mater.*, vol. 273, p. 121739, 2021, doi: 10.1016/j.conbuildmat.2020.121739.

[45] J.-H. Zhu, Z. Wang, M. Su, T. Ueda, and F. Xing, “C-FRCM Jacket Confinement for RC Columns under Impressed Current Cathodic Protection,” *J. Compos. Constr.*, vol. 24, no. 2, p. 04020001, 2020, doi: 10.1061/(asce)cc.1943-5614.0001006.

[46] L. Ombres and S. Verre, “Structural behaviour of fabric reinforced cementitious matrix (FRCM) strengthened concrete columns under eccentric loading,” *Compos. Part B Eng.*, vol. 75, pp. 235–249, 2015, doi: 10.1016/j.compositesb.2015.01.042.

[47] N. Tello, Y. Alhoubi, F. Abed, A. El Refai, and T. El-Maaddawy, “Circular and square columns strengthened with FRCM under concentric load,” *Compos. Struct.*, vol. 255, no. September 2020, p. 113000, 2021, doi: 10.1016/j.compstruct.2020.113000.

[48] American Concrete Institute (ACI), *Building code requirements for structural concrete and commentary*, ACI 318-19. Farmington Hills, MI, USA: American Concrete Institute, 2019.

[49] ASTM C39 / C39M-20, *Standard Test Method for Compressive Strength of Cylindrical Concrete Specimens*. West Conshohocken, PA: ASTM International, 2020.

[50] British Standard Institution, *Testing concrete method for determination of compressive strength of concrete cubes*, BS 1881-116:1983. London: BSI, 1983.

[51] ASTM A370, *Standard Test Methods and Definitions for Mechanical Testing of Steel Products*. West Conshohocken, PA: ASTM International, 2019.

[52] M. J. Shannag and M. A. Alhassan, "Seismic upgrade of interior beam-column subassemblages with high-performance fiber-reinforced concrete jackets," *ACI Struct. J.*, vol. 102, no. 1, pp. 131–138, 2005, doi: 10.14359/13538.

Vita

Nour Al Huda Haitham Tello was born in 1998, in Abu Dhabi, United Arab Emirates. She received her primary and secondary education from Rosary School in Abu Dhabi. After graduating high school, she joined the American University of Sharjah (AUS) in September 2015 and graduated Cum Laude with a Bachelor of Science in Civil Engineering degree in June 2019. In September 2019, she returned to AUS to join the Civil Engineering master's program after receiving a graduate research assistantship. During her master's study, she co-authored a total of four conference and journal papers and has presented in a number of local and international conferences. Her research interests are mainly in structural engineering and materials.